NASA TECHNICAL MEMORANDUM 107704

THREE-DIMENSIONAL ELASTIC-PLASTIC FINITE-ELEMENT ANALYSES OF CONSTRAINT VARIATIONS IN CRACKED BODIES

J. C. Newman, Jr., C. A. Bigelow
and K. N. Shivakumar

JANUARY 1993

National Aeronautics and
Space Administration
Langley Research Center
Hampton, Virginia 23681-0001

THREE-DIMENSIONAL ELASTIC-PLASTIC FINITE-ELEMENT ANALYSES OF CONSTRAINT VARIATIONS IN CRACKED BODIES

J. C. Newman, Jr.[1], C. A. Bigelow[1] and K. N. Shivakumar[2]

NASA Langley Research Center

Hampton, Virginia

ABSTRACT

Three-dimensional elastic-plastic (small-strain) finite-element analyses were used to study the stresses, deformations, and constraint variations around a straight-through crack in finite-thickness plates for an elastic-perfectly plastic material under monotonic and cyclic loading. Middle-crack tension specimens were analyzed for thicknesses ranging from 1.25 to 20 mm with various crack lengths. Three local constraint parameters, related to the normal, tangential, and hydrostatic stresses, showed similar variations along the crack front for a given thickness and applied stress level. Numerical analyses indicated that cyclic stress history and crack growth reduced the local constraint parameters in the interior of a plate, especially at high applied stress levels. A global constraint factor α_g was defined to simulate three-dimensional effects in two-dimensional crack analyses. The global constraint factor was calculated as an average through-the-thickness value over the crack-front plastic region. Values of α_g were found to be nearly independent of crack length and were related to the stress-intensity factor for a given thickness.

---

1 NASA Langley Research Center, Hampton, VA 23681-0001

2 North Carolina A&T State University, Greensboro, NC 27410

Using the global constraint factors, crack-tip opening displacements calculated from a modified Dugdale model compared well with the finite-element results from small- to large-scale yielding conditions for both thin and thick bodies. An application of the global constraint factor concept to model fatigue-crack growth under aircraft spectrum loading is presented.

INTRODUCTION

The importance of "constraint" in the analysis of notched or cracked bodies has long been recognized by many investigators. Constraint refers to the buildup of stresses around a crack front due to the restraint against in-plane and out-of-plane deformation. Out-of-plane constraint is mainly influenced by plate thickness whereas in-plane constraint has been associated with the closeness of the crack front to external boundaries. The level of constraint depends upon the crack configuration and thickness, the type and magnitude of applied load, and the material stress-strain properties. The level of constraint influences fatigue-crack growth and fracture behavior of a cracked body. In the field of fracture mechanics, constraint has often been used only in a qualitative manner, such as plane-stress or plane-strain constraint. In the last few years, however, a concerted effort by the fracture community (see for example, refs. 1 and 2) has been undertaken to quantify the influence of constraint on fracture. To evaluate various constraint parameters, two and three-dimensional stress analysis methods have been used to determine stress and deformation states for cracked bodies.

In the past, Levy, Marcal, and Rice [3], Kiefer and Hilton [4], de Lorenzi and Shih [5], and Moyer and Liebowitz [6] used three-dimensional, small-strain, finite-element analyses to study cracked finite-thickness plates. Sih and Chen [7] used small-strain plasticity theory but departed from classical approaches by varying the tensile flow properties through the

thickness. Brocks et.al [8] and Hom and McMeeking [9] used large-strain, finite-element analyses to study the local stresses and deformations around a crack in finite-thickness plates. Similar analyses were also carried out by Wilkins [10] and Ayres [11] using finite-difference methods and by Malik and Fu [12] with the method of lines. All of these investigators obtained plastic-zone shapes and stress distributions around the crack front for specific crack configurations.

More recently, the T stress (the tangential stress that is in-plane and parallel to the crack surfaces [13]), and the Q stress (a stress factor used to characterize the difference between the actual stresses and the HRR stress field [14]) were used as in-plane constraint parameters for two-dimensional cracked bodies. Analyses by Brocks and Kunecke [15], and analyses and tests by Sommer and Aurich [16], on laboratory specimens and on surface-crack configurations showed how constraint (in particular, the mean-stress-to-equivalent-stress ratio, σ_m/σ_v) affected stable crack-growth behavior under monotonic loading.

Fatigue-crack growth in metallic materials is also influenced by constraint variations around the crack front. A constraint parameter based on the normal-stress-to-flow-stress ratio (σ_{yy}/σ_0) was used to characterize fatigue crack-growth and crack-closure behavior under cyclic loading [17,18].

The transfer of fatigue-crack-growth and fracture data from laboratory specimens to structural configurations depends upon the ability to calculate and match the constraint parameters with the appropriate crack-driving parameters (K, J or δ). A parametric study on the influence of configuration, thickness, crack length, and applied stress level on crack-front stresses, deformations, and constraint for standard laboratory

specimens and common crack configurations found in practice is lacking in the literature. Because of the complex stress fields, these studies must be conducted using three-dimensional numerical stress analyses. From these analyses, expressions characterizing constraint need to be developed. Given a body with a through-the-thickness crack, as shown in Figure 1, equations need to be developed which express the crack-front constraint as a function of configuration, loading, and material properties as

$$\text{Constraint} = f(c, w, B, S, E, \sigma_0, n) \tag{1}$$

where c is the crack length, w is width, B is thickness, S is the applied stress, E is the modulus of elasticity, σ_0 is the uniaxial flow stress, and n is the strain-hardening coefficient. These expressions may then be used to characterize fatigue-crack-growth and fracture behavior under various constraint conditions or they may be used in two-dimensional models, such as the modified Dugdale model, to correlate and predict fatigue-crack growth [17] and fracture [19]. For use in two-dimensional models, however, an average through-the-thickness constraint factor may be required.

Fatigue-crack growth and fracture tests on metallic materials have shown that shear lips develop during the transition from a flat to a slant type of crack growth, as shown in Figure 2. This transition has long been associated with a constraint loss but the stress states corresponding to this transition have not been quantified. Schijve [20] and others have also shown that the transition during fatigue-crack growth is strongly influenced by environment.

The objective this paper is to present detailed three-dimensional elastic-plastic, finite-element results on the influence of crack length, plate thickness, type of loading and load level on the triaxial constraint variations for a straight-through crack front in an elastic-perfectly

plastic material. A standard laboratory middle-crack tension specimen was analyzed. Primarily, monotonic loading with a stationary crack front was considered but a thin specimen was also analyzed under cyclic loading with crack extension. Although stable tearing under monotonic loading is of interest, constraint variations under stable tearing will not be studied here. Results under cyclic loading, however, may indicate some of the trends that would be observed for stable tearing under monotonic loading. Some numerical results for out-of-plane deformation will also be compared with experiments and another numerical analysis from the literature.

Three "local" constraint parameters related to the normal, tangential, and hydrostatic stress states will be compared for various crack lengths and plate thicknesses. These three constraint parameters were selected because they have been used in the literature to characterize constraint behavior for either fatigue-crack growth or fracture behavior. A "global" constraint factor α_g was also defined for use in two-dimensional crack analyses to simulate three-dimensional effects. The global constraint factor was defined as the average through-the-thickness value of constraint over the plastic-zone region. Using the global constraint factor, the crack-tip opening displacements from a modified Dugdale model [17] were compared with the present three-dimensional results from small- to large-scale yielding conditions. An application of the global constraint factor concept to model fatigue-crack growth under aircraft spectrum loading is presented.

NOMENCLATURE

B Plate thickness, m

c Crack half-length, m

d Minimum element size in crack-front region, m

E Modulus of elasticity, MPa

h	Plate half-height, m
K	Mode I (two-dimensional) stress-intensity factor, MPa-$\sqrt{m}$
n	Strain-hardening coefficient
R	Stress ratio (S_{min}/S_{max})
S	Applied stress, MPa
S_{max}	Maximum applied stress, MPa
S_{min}	Minimum applied stress, MPa
S_{mf}	Mean-flight stress level in TWIST spectrum, MPa
u_z	Displacement in z-direction, m
v	Crack-opening displacement at specified distance from crack front, m
v_o	Crack-opening displacement, v, at mid-plane ($y = z = 0$), m
w	Plate half-width, m
x,y,z	Cartesian coordinates
α	Ratio of σ_{yy}/σ_o along crack front
α_g	Global constraint factor based on σ_{yy} for yielded material on uncracked ligament
ΔK_{eff}	Effective (closure-corrected) stress-intensity factor range, MPa-$\sqrt{m}$
δ_{45}	Crack-tip opening displacement at 45 degree intercept location, m
ν	Poisson's ratio
σ_{ij}	Stress tensor, MPa
σ_m	Hydrostatic stress $(\sigma_{xx}+ \sigma_{yy}+ \sigma_{zz})/3$, MPa
σ_o	Uniaxial flow stress, MPa
σ_v	Equivalent stress (proportional to octahedral shear stress), MPa
T	Ratio of σ_{xx}/σ_o along crack front

χ Ratio of σ_m/σ_0 along crack front

CRACK CONFIGURATION, MATERIAL AND LOADING

The middle-crack tension specimen was analyzed for thicknesses (B) ranging from 1.25 to 20 mm with crack-half-length-to-specimen-half-width (c/w) ratios of 0.3, 0.5 and 0.7 (w = 40 mm). Plane-strain conditions were also imposed on some finite-element models to show limiting conditions. The material was assumed to be elastic-perfectly plastic with properties typical of a high-strength aluminum alloy. The modulus of elasticity (E) was selected to be 71,500 MPa, the flow stress (σ_0) was 500 MPa (unless otherwise stated), and Poisson's ratio (ν) was 0.3. The finite-element models were subjected to either monotonic or cyclic loading. Under monotonic loading, the crack front was held stationary, but under cyclic loading, the crack was grown uniformly through the thickness by one element size at the maximum applied stress in each cycle. During unloading, the closure of the crack surfaces with contact stresses was modeled.

FINITE-ELEMENT ANALYSES

A three-dimensional (3D), elastic-plastic, finite-element program, ZIP3D [21], developed at the NASA Langley Research Center, was used in this study. The program uses 8-noded hexahedral elements, the von Mises yield criterion, isotropic hardening, small-strain deformation theory, and the associated flow rule. The numerical algorithm is based on the initial-stress method and incremental theory of plasticity [22]. Crack extension and closure under cyclic loading are modeled by nodal-release and contact procedures [23].

The 3D finite-element model, as shown in Figure 3, contained six layers through the half-thickness. The layer adjacent to the mid-plane of the specimen (along the x-y plane) is denoted as Layer 1. Thicknesses of Layers

1 to 6 were 0.15, 0.125, 0.1, 0.0625, 0.0375 and 0.025 of B, respectively. Figure 3 shows the model for a specimen with c/w = 0.5. For all cases, the specimen half-width, w, was selected to be 40 mm and the half-height, h, was 80 mm. Region 1 shows the mesh refinement around the crack front. The smallest element size, d, in the crack-front region (Region 1) was about 0.03 mm. For c/w ratios of 0.3 and 0.7, the model shown in Figure 3 was modified by expanding or contracting elements in the regions $x < 0.4w$ and $x > 0.6w$ to achieve the required c/w ratio. Therefore, the region around the crack front ($0.4w \leq x \geq 0.6w$) was shifted but the element sizes and pattern were left unchanged. All models had the same number of elements (5,706) and nodes (7,203). A uniform displacement was applied across the y = h plane. In the incremental analysis, the displacement increment selected was thirty percent of the displacement required to yield the highest stressed element. The analyses were conducted on a super-computer and the analysis of each crack configuration was terminated when the plastic-yield region extended across the net-section.

RESULTS AND DISCUSSION

As previously mentioned, three "local" constraint parameters along the crack front are examined and compared for various thicknesses. These parameters were based on the normal, tangential, and hydrostatic stresses along the crack front. The normal-stress constraint factor is defined as the ratio of the normal stress to the flow stress (σ_{yy}/σ_0) along the crack front and is denoted as α. The tangential-stress constraint factor is defined as the ratio of the tangential stress to the flow stress, denoted as $T = \sigma_{xx}/\sigma_0$. Similarly, the hydrostatic constraint factor is defined as $\chi = \sigma_m/\sigma_0$ where σ_m is the hydrostatic stress. The variation of these parameters along the crack front with different specimen thicknesses, crack lengths and

applied stress-intensity factor levels is presented. In addition, a "global" constraint factor α_g is defined as the average normal-stress-to-flow-stress ratio acting over the yielded elements on the uncracked ligament. A comparison of the global constraint factor under monotonic and cyclic loading is made. Some results on the influence of constraint on fatigue-crack growth under aircraft spectrum loading are presented and discussed.

Monotonic Loading

Stress State.-The normal stress, σ_{yy}, in the crack-front region normalized by the flow stress, σ_0, is shown in Figures 4 and 5 for a thick and thin specimen (B = 10 and 2.5 mm), respectively. The ratio of crack half-length to half-width (c/w) was 0.5. Centroidal stresses along the crack plane are plotted for Layers 1 to 6 as a function of x/c, where the crack front is located at x/c = 1. These results are shown for specific values of the applied normalized stress-intensity factor, $K/(\sigma_0\sqrt{w})$, where K is the two-dimensional stress-intensity factor. K was calculated from the well-known formula for the middle-crack tension specimen [24]. For the thick specimen (Fig. 4), the normal-stress ratio remained high (about 2.8) at the crack front for all layers except the surface layer (Layer 6). However, in the thin material (Fig. 5), the stresses at the crack front dropped noticeably in each layer, indicating a loss of local constraint. The normal-stress ratio also dropped rapidly for elements away from the crack front. The peak values of normal stress at the mid-plane of the plates and variations through the thickness from the present analyses compared well with those from Kiefer and Hilton [4] and Moyer and Liebowitz [6]. The dashed line shows the global constraint factor, α_g, which is the

average σ_{yy}/σ_0 for all yielded material on the uncracked ligament (discussed later in Global Constraint Factor section). The value of α_g is lower for the thinner material indicating less constraint than the thicker material.

The variation of the local constraint, α, along the crack front for thicknesses of 1.25, 5 and 20 mm is shown in Figure 6 as a function of z/B. The mid-plane of the plate is at z/B = 0 and the free surface is at z/B = 0.5. The c/w ratio was 0.5 and the applied normalized stress-intensity factor level was 0.33. The thickest material (B = 20 mm) showed a nearly constant value of α through the thickness, with a slight rise and then a sharp drop near the free surface (z/B = 0.5). However, the thinnest material (B = 1.25 mm) showed a more gradual drop in α from the center of the sheet (z/B = 0) to the free surface.

To show the variation of the three local constraint parameters (α, T and χ) through the thickness, each parameter was normalized by its value at the mid-plane of the plate. The parameters are given by

$$\bar{\alpha} = \sigma_{yy}(z)/\sigma_{yy}(0)$$

$$\bar{T} = \sigma_{xx}(z)/\sigma_{xx}(0)$$

and $$\bar{\chi} = \sigma_m(z)/\sigma_m(0)$$

The variation of $\bar{\alpha}$ and $\bar{T}$ with z/B for several thicknesses is shown in Figure 7 for c/w = 0.5 and $K/(\sigma_0\sqrt{w}) = 0.33$. Although $\bar{\alpha}$ and $\bar{T}$ show similar trends, $\bar{T}$ varied more across the plate thickness than $\bar{\alpha}$. Figure 8 shows the variation of $\bar{\alpha}$ and $\bar{\chi}$ for the same configuration and loading. Both $\bar{\alpha}$ and $\bar{\chi}$ showed nearly identical trends.

The local constraint parameters α and χ at the mid-plane for three different thicknesses is shown in Figure 9 as a function of applied stress-intensity factor level. Both parameters are nearly independent of specimen thickness and increase as the applied stress-intensity factor level, $K/(\sigma_0\sqrt{w})$, is increased up to about 0.5. Thereafter, the constraint parameters drop with increasing stress-intensity factor levels but show a sharp rise at $K/(\sigma_0\sqrt{w}) \approx 0.8$ which corresponds to the yield zone extending across the uncracked ligament. Again, the parameters α and χ showed the same trends but, of course, at different magnitudes; the trends in T are also similar.

Global Constraint Factor.-The global constraint factor was developed in the present study for use with existing two-dimensional models [17,19] of crack-growth behavior to approximately account for the effects of three-dimensional stress state on crack-surface displacements. These models, which are based on the Dugdale model [25], require a constant stress in the tensile plastic zone. Thus, an average of the normal stresses acting over the yielded material on the uncracked ligament may be an appropriate value to calculate a constraint parameter. The global constraint factor is, thus, defined as

$$\alpha_g = \frac{1}{A_T} \sum_{m=1}^{M} (\sigma_{yy}/\sigma_0)_m \, A_m \qquad (2)$$

where A_m is the projected area on the uncracked ligament of a yielded element m, $(\sigma_{yy}/\sigma_0)_m$ is the normalized normal stress for element m, and A_T is the total projected area for all elements (M) which have yielded.

The variation of α_g with applied stress-intensity factor level for a wide range of plate thicknesses (B = 1.25 to 20 mm) is shown in Figure 10

for a c/w ratio of 0.5. Results for plane-strain conditions are also shown for comparison and indicate a limiting solution. The dash-dot line at α_g = 1 also denotes a lower limit under uniaxial stress conditions. The portion of the curves shown as dashed lines were considered invalid because less than four elements were yielded in Layer 1. The solid curves show a loss in global constraint as the applied K level (or equivalently the plastic-zone size) increases. For a given K level, the thinner specimens gave the lowest constraint factors. Results for all thicknesses tended to approach nearly the same constraint level (about 1.15) as large-scale yielding conditions were reached. The upper solid curve, the plane-strain solution, shows a much slower constraint loss with increasing K level. Again, the rapid loss of constraint at $K/(\sigma_0\sqrt{w})$ of about 0.9 was associated with the extension of the plastic region across the uncracked ligament. The flow stress used for these comparisons was 500 MPa. However, some calculations made with σ_0 equal to 300 and 700 MPa for various thicknesses (not shown) demonstrated that the normalized stress-intensity factor $K/(\sigma_0\sqrt{w})$ was able to collapse the results for various flow stresses onto the same curves.

Figure 11 shows the effect of crack length on the global constraint factors for the same range of thicknesses as previously shown. The constraint factors were nearly independent of crack length for the range of thicknesses considered, especially for the thin sheets. For the two largest c/w ratios 0.5 and 0.7, α_g was nearly identical for all thicknesses. Some slight differences were observed for large-scale yielding conditions. For the thicker plates, the results for a c/w ratio of 0.3 were slightly lower (less than 5 percent) than the results for the other c/w ratios. Again, the limiting uniaxial stress condition (α_g = 1) is shown by the dash-dot line.

Deformations.-The variations of the normalized crack-tip-opening displacements along the crack front are shown in Figures 12 and 13 for the applied normalized stress-intensity factor levels of 0.33 and 0.66, respectively. Crack-tip-opening displacement (v) is defined as the displacement at the second node behind the crack front (0.06 mm behind the crack front or x/c = 0.9968). The displacements were normalized by the displacement (v_0) at the mid-plane (z/B = 0). Results for three different thicknesses (B = 1.25, 5 and 20 mm) are shown in each figure. For $K/(\sigma_0\sqrt{w})$ = 0.33 (Fig. 12), the normalized displacements were nearly constant through the thickness, except for some slight variations near the free surface (less than 10 percent). However, for the higher applied stress-intensity factor level (Fig. 13), significant variations in displacement through the thickness were calculated. At both applied stress-intensity factor levels, the results for the thick specimens showed a drop in displacement near the free surface, whereas the results for the thin specimen showed a rise in displacement at the free surface. Crack-surface displacements calculated at locations farther from the crack front (x/c < 0.9968) showed less variation through the thickness, as expected.

Figure 14 shows the crack-tip-opening displacement (v_0) at the mid-plane (z/B = 0) of the specimen normalized by the crack length and plotted against the applied stress-intensity factor level. Again, displacements are shown for the second node behind the crack front (x/c = 0.9968). Finite-element method (FEM) results are shown for the thinnest and thickest plates analyzed (symbols). For the same applied stress-intensity factor, v_0 is larger for the thinner specimen. As expected, the thinnest specimen has a lower overall constraint and, hence, has larger displacements near the crack front compared to the thicker specimen. The plane-stress elastic solution

is shown by the lowest dash curve. The finite-element results for $K/(\sigma_0\sqrt{w})$ < 0.1 generally were within 2 percent of the elastic solution. The solid curves show the calculated crack-tip-opening displacements (at x/c = 0.9968) using the modified Dugdale model (MDM) [17] with the α_g values calculated from the 3D finite-element analyses (as shown in Fig. 10). The effective flow stress in the MDM was $\alpha_g\sigma_0$. The solid curves agreed reasonably well with the finite-element results from small- to large-scale yielding conditions. Some differences were observed for the thick material for $K/(\sigma_0\sqrt{w})$ greater than 0.7. The upper and middle dashed curves in Figure 14 show the solutions from the MDM for α_g = 1 and 3. At low values of applied $K/(\sigma_0\sqrt{w})$, the FEM and MDM results approached the plane-strain solution. However, at high values of applied $K/(\sigma_0\sqrt{w})$, the FEM results showed a loss of constraint. The vertical asymtote from the FEM results would be predicted from the MDM using an α_g value of about 1.1 for the thin specimen and 1.2 for the thick specimen. These results suggest that the global constraint factor controls the crack-surface displacements very close to the crack front and that the MDM can be used to model three-dimensional effects.

A comparison of out-of-plane displacements from analyses and tests for a thin-sheet specimen is shown in Figure 15. The displacement in the z-direction, u_z, was calculated at the free surface along the crack plane (y = 0 and z = B/2) and plotted against the normalized distance from the crack front, (x-c)/B. The present results are shown as the solid curve (E/σ_0 = 238; n = 0) for B = 2.5 mm. (Note that the flow stress was selected as 300 MPa for these comparisons.) Results from Hom and McMeeking [9] using a finite-deformation analysis of a very sharp notch in a strain-hardening

material (E/σ_0 = 100; n = 0.1) are shown as the dashed curve. Experimental measurements from Chiang and Hareesh [26] on a sharply-notched specimen made of 6061-T6 aluminum alloy (E/σ_0 = 246; n = 0.054) with B = 3.2 mm are shown by the symbols. All out-of-plane displacements were normalized by the crack-tip-opening displacement at the 45 degree intercept (δ_{45}). All results agreed quite well for (x-c)/B values greater than about 0.5. However, large differences between the three results were found near the crack front, a highly deformed region. The large out-of-plane deformation gradient around the crack front clearly illustrates the cause of high constraint. The material along the crack surfaces, which does not yield, restrains the material ahead of the crack front causing a large buildup of the σ_{zz} stresses through the thickness and, therefore, constraint. These stresses and out-of-plane deformations decrease sharply for locations away from the crack front.

For monotonic loading with stable crack extension, the deformed material in the wake of the crack front would be expected to reduce the deformation gradient at the crack front and cause a lower constraint. A study on stable crack extension, however, would involve a fracture criterion and this is beyond the scope of the present paper. Further research on the influence of stable crack extension and the plastic wake on constraint is needed. A previous study [23] using a 3D finite-element analysis of crack growth under cyclic loading did not use a failure criterion but allowed the crack to grow only at maximum load. Therefore, the influence of crack extension under cyclic loading on constraint will be briefly studied here.

Cyclic Loading

Cracks growing under cyclic loading leave residual plastic deformations along the crack surfaces. Therefore, the constraint around a crack front

may be influenced by the deformation history. To study this behavior, a finite-element model of a thin (B = 2.5 mm) specimen was subjected to cyclic loading at various maximum applied stress-intensity factor levels with the minimum stress-intensity factor equal to zero (R = 0). During each cycle, the crack front was arbitrarily extended one element size (0.03 mm) at the maximum stress-intensity factor level. During unloading, the crack surfaces were allowed to close and carry compressive contact stresses [23]. Five cycles were applied to each specimen and the final crack length was equal to the crack length used in the monotonic loading cases.

Stress State.-Comparisons of local normal stress states under cyclic and monotonic loading in the B = 2.5 mm thick specimen are shown in Figures 16 and 17 for two levels of applied stress-intensity factors. Stresses are plotted ahead of the crack front for Layers 1, 4 and 6. At the $K/(\sigma_0\sqrt{w})$ = 0.33 level, the normal stresses were nearly the same for both monotonic and cyclic loading. A slight drop in stresses did occur along the crack front in the interior under cyclic loading. But the stresses away from the crack front under cyclic loading were equal to or slightly higher than those under monotonic loading. In contrast, the behavior under the higher applied K level (Fig. 17) showed a large reduction in local stresses in the interior of the plate (Layer 1). These results show that the cyclic stress history and crack extension can have a strong influence on the local stresses.

Global Constraint Factor.-The global constraint factors, α_g, under monotonic and cyclic loading are compared in Figure 18 for the B = 2.5 mm thick material as a function of the applied stress-intensity factor level. The symbols show the results of four cyclic crack-growth analyses conducted at different maximum stress-intensity factor levels with R = 0. Results from the monotonic loading (from Fig. 10) are shown as the solid curve. The

α_g values under cyclic loading were slightly higher than those from monotonic loading for low cyclic K levels, presumably because the normal stresses away from the crack front were slightly higher than those under monotonic loading. The results at the higher cyclic K levels, however, agreed very well with the results from monotonic loading, even though the local stresses in the interior (Layer 1) were substantially lower under cyclic loading (as shown in Fig. 17). The same α_g values may have been caused, in part, by the other layers carrying equal or slightly higher stresses under cyclic loading than under monotonic loading. The dashed-dot line shows an assumed constraint-loss regime from a previous study which correlated fatigue-crack growth rates under constant-amplitude loading and calculated crack growth under an aircraft spectrum loading [27]. The material studied in reference 27 was 2024-T3 Alclad aluminum alloy with a thickness of 3.1 mm. The constraint-loss regime defines the region where a drop in constraint occurs, such as from plane-strain to plane-stress conditions. The constraint-loss (or variable-constraint) regime was selected in reference 27 to roughly correspond to the transition region where crack growth changes from flat to slant, as illustrated previously in Figure 2. Results from the present and future studies on constraint may eventually provide the means to calculate the constraint-loss regime.

Applications to Fatigue Crack Growth

Constraint has a strong influence on fatigue-crack growth and crack-closure behavior of metallic materials [17,18]. To illustrate this influence, the constraint-loss regime (dash-dot curve) shown in Figure 18 was used to calculate crack growth under an aircraft spectrum loading.

Wanhill [28] conducted spectrum crack-growth tests on middle-crack tension specimens made of 2024-T3 Alclad material (B = 3.1 mm). Tests were

conducted under the TWIST [29] spectrum clipped at Level III with a mean flight stress, S_{mf} = 70 MPa. The initial crack starter notch half-length was 3.5 mm. Comparisons are made here between experimental and calculated crack length against flights for TWIST (Level III) loading. Other comparisons are given in reference 27.

Crack-length-against-flight data for the 3.1 mm-thick specimens tested under the TWIST (Level III) loading are shown in Figure 19. The figure shows experimental results (symbols) from two separate specimens tested under identical conditions. The solid curve is the calculated results from the closure model with the variable-constraint condition (α_g = 2 to 1, as shown in Fig. 18) using a baseline ΔK_{eff}-rate relation determined from constant-amplitude data [27]. The calculated results agreed well with the tests, within 15 percent on flights to a given crack length.

To illustrate why the variable-constraint conditions are necessary, calculations were made for constant constraint conditions of either α_g = 1 or 2 (dashed-dot curves). The model with a low constraint condition (α_g = 1) predicted much longer flights to a given crack length than the test data. Conversely, the predicted results for the higher constraint condition (α_g = 2) greatly under-predicted the behavior except in the early stages of growth. If the material had been tested at a mean-flight stress level lower than 70 MPa, it is expected that the lives would have fallen closer to the calculations made with α_g = 2 because the higher constraint condition would have been applied during more of the life time. In contrast, tests conducted at a higher mean-flight stress level may have fallen closer to the calculated results using α_g = 1.

CONCLUSIONS

Three-dimensional elastic-plastic (small-strain) finite-element analyses were used to study the stresses and deformations around a straight-through crack in finite-thickness plates for an elastic-perfectly plastic material under monotonic and cyclic loading. For monotonic loading, the crack front was held stationary, whereas under cyclic loading the crack front was grown at maximum stress conditions. Three "local" crack-front constraint parameters related to the normal, tangential, and hydrostatic stresses were compared for middle-crack tension plates ranging from 1.25 to 20 mm thick with various crack lengths. Plane-strain solutions were also obtained. A "global" constraint factor, an average through-the-thickness value, was defined for use with the modified Dugdale model. Crack-opening displacements near the crack front were compared with a modified Dugdale model for various thicknesses and applied stress levels. Through-the-thickness deformations were also compared with experimental and numerical results from the literature. The results of this study support the following conclusions:

(1) Commonly used constraint parameters defined for multiaxial stress states show similar variations along the crack front and with applied stress-intensity factor levels for stationary cracks.

(2) All plate thicknesses considered (B = 1.25 to 20 mm) developed a large amount of local constraint in the interior regions even under large-scale plastic yielding for stationary cracks.

(3) Cyclic stress history and crack growth reduced the local constraint in the interior of a plate, especially under high applied stress-intensity factor levels.

(4) The global constraint factor (α_g) was nearly the same for a given stress-intensity factor for various crack lengths and flow stresses from small- to large-scale yielding.

(5) For a given applied stress-intensity factor level, thinner specimens developed lower global constraint factors that the thicker specimens.

(6) Using the global constraint factors, the crack-opening displacements calculated from the modified Dugdale model agreed reasonably well with the three-dimensional, finite-element displacements calculated in the interior of finite-thickness specimens.

(7) Using a variable constraint factor improved fatigue-crack-growth calculations under the TWIST aircraft spectrum loading.

REFERENCES

[1] Blauel, J. G. and Schwalbe, K. -H., eds., Defect Assessment in Components - Fundamentals and Application, ESIS/EGF 9, Mechanical Engineering Publications, Ltd. (1991).

[2] Hackett, E., Schwalbe, K.-H. and Dodds, R., eds., Constraint Effects in Fracture, ASTM STP 1171 (1993).

[3] Levy, N., Marcal, P. V. and Rice, J., Progress in Three-Dimensional Elastic-Plastic Stress Analysis for Fracture Mechanics. Nuclear Engng. Design 17, 64-75 (1971).

[4] Kiefer, B. V. and Hilton, P. D., Three-Dimensional Finite Element Analysis of Elastic-Plastic Crack Problems. J. Pressure Vessel Tech. 103, 214-218 (1981).

[5] de Lorenzi, H. G. and Shih, C. D., 3-D Elastic-Plastic Investigation of Fracture Parameters in Side-Grooved Compact Specimen. Int. J. Fracture 21, 195-220 (1983).

[6] Moyer, E., Jr. and Liebowitz, H., Effect of Specimen Thickness on Crack Front Plasticity Characteristics in Three Dimensions, Advances in Fracture Research (Fracture 84), Pergamon Press, 889-896 (1986).

[7] Sih, G. C. and Chen, C., Non-self-similar Crack Growth in Elastic-Plastic Finite Thickness Plate. Theoretical and Applied Fracture Mechanics 3, 125-139 (1985).

[8] Brocks, W., Muller, W. and Olschewski, J., Experiences in Applying ADINA to the Analysis of Crack Tip Fields in Elastic-Plastic Fracture Mechanics. Computers and Structures 21, 137-158 (1985).

[9] Hom, C. L. and McMeeking, R. M., Large Crack Tip Opening in Thin Elastic-Plastic Sheets. Int. J. Fracture 45, 103-122 (1990).

[10] Wilkins, M. L., Calculation of Elastic-Plastic Flow, Report TID-4500, UC 34, Lawrence Livermore Laboratory (1969).

[11] Ayres, D. J., A Numerical Procedure for Calculating Stress and Deformation Near a Slit in a Three-Dimensional Elastic-Plastic Solid. Engng. Fracture Mechanics 2, 87-106 (1970).

[12] Malik, S. N. and Fu, L. S., Elasto-Plastic Analysis for a Finite Thickness Rectangular Plate Containing a Through-Thickness Central Crack. Int. J. Fracture 18, 45-63 (1982).

[13] Hancock, J. W., Reuter, W. G. and Parks, D. M., Constraint and Toughness Parameterised by T. ASTM Symposium on Constraint Effects in Fracture, Indianapolis, IN (1991).

[14] O'Dowd, N. P. and Shih, C. F., A Family of Crack Tip Fields Characterized by a Triaxiality Parameter. Submitted to J. Mech. Phys. Solids (1992).

[15] Brocks, W. and Kunecke, G., On the Influence of Triaxiality of the Stress State on Ductile Tearing Resistance, Defect Assessment in Components - Fundamentals and Applications, ESIS/EGF 9, J. G. Blauel

and K. -H. Schwalbe, eds., Mechanical Engineering Publication, 189-201 (1991).

[16] Sommer, E. and Aurich, D., On the Effect on Constraint on Ductile Fracture, Defect Assessment in Components - Fundamentals and Applications, ESIS/EGF 9, J. G. Blauel and K. -H. Schwalbe, eds., Mechanical Engineering Publication, 141-174 (1991).

[17] Newman, J. C., Jr., A Crack-Closure Model for Predicting Fatigue Crack Growth under Aircraft Spectrum Loading, Methods and Models for Predicting Fatigue Crack Growth under Random Loading, ASTM STP 748, J. B. Chang and C. M. Hudson, eds., 53-84 (1981).

[18] McClung, R. C. and Sehitoglu, H., Constraint Effects in Fatigue Crack Growth, Proceedings 3rd Int. Conf. Fatigue and Fatigue Thresholds, Charlottesville, VA, 1401-1410 (1987).

[19] Newman, J. C., Jr., Prediction of Stable Crack Growth and Instability Using the V_R-Curve Method, Elastic-Plastic Fracture Mechanics Technology, ASTM STP 896, J. C. Newman, Jr. and F. J. Loss, eds., 139-166 (1985).

[20] Schijve, J., Jacobs, F. A. and Tromp, P. J., Environmental Effects on Crack Growth in Flight-Simulation Tests on 2024-T3 and 7075-T6 Material, NLR-TR 76104 U, National Aerospace Laboratory (1976).

[21] Shivakumar, K. N. and Newman, J. C., Jr., ZIP3D - An Elastic and Elastic-Plastic Finite-Element Analysis Program for Cracked Bodies, NASA TM 102753 (1990).

[22] Zienkiewicz, O. C., Valliappan, S., and King, I. P., Elasto-Plastic Solutions of Engineering Problems, Initial Stress, Finite-Element Approach. Int. J. Numerical Methods in Engng. 1, 75-100 (1969).

[23] Chermahini, R. G., Shivakumar, K. N. and Newman, J. C., Jr., Three-Dimensional Finite-Element Simulation of Fatigue Crack Growth and Closure, Mechanics of Fatigue Crack Closure, ASTM STP 982, J. C. Newman, Jr. and W. Elber, eds., 398-413 (1988).

[24] Tada, H., Paris, P. C. and Irwin, G. R., The Stress Analysis of Cracks Handbook, Del Research Corp. (1985).

[25] Dugdale, D. S., Yielding of Steel Sheets Containing Slits. J. Mech. Phys. Solids 8, 100-104 (1960).

[26] Chiang, F. P. and Hareesh, T. V., Three-Dimensional Crack-Tip Deformation: An Experimental Study and Comparison to HRR Field. Int. J. Fracture 36, 243-257 (1988).

[27] Newman, J. C., Jr., Effects of Constraint on Crack Growth under Aircraft Spectrum Loading, Fatigue of Aircraft Materials, Delft University Press, The Netherlands, 83-109 (1992).

[28] Wanhill, R. J. H., Flight Simulation Fatigue Crack Propagation Evaluation of Candidate Lower Wing Skin Materials with Particular Consideration of Spectrum Truncation, NLR TR 77092 U (1977).

[29] de Jonge, J. B., Schutz, D., Lowak, H. and Schijve, J., A Standardized Load Sequence for Flight Simulation Tests on Transport Aircraft Wing Structures, LBF-Bericht FB-106, NLR TR 73029 U (1973).

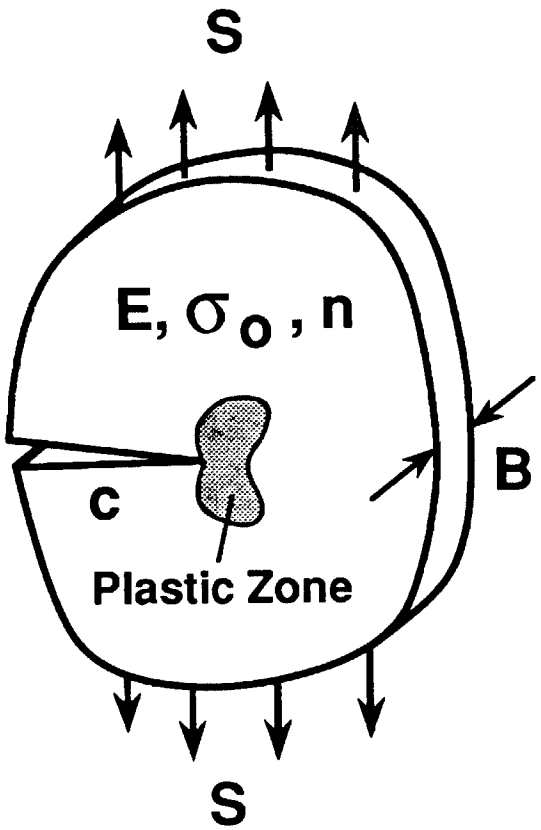

Figure 1.- Crack in finite-thickness plate with plastic zone.

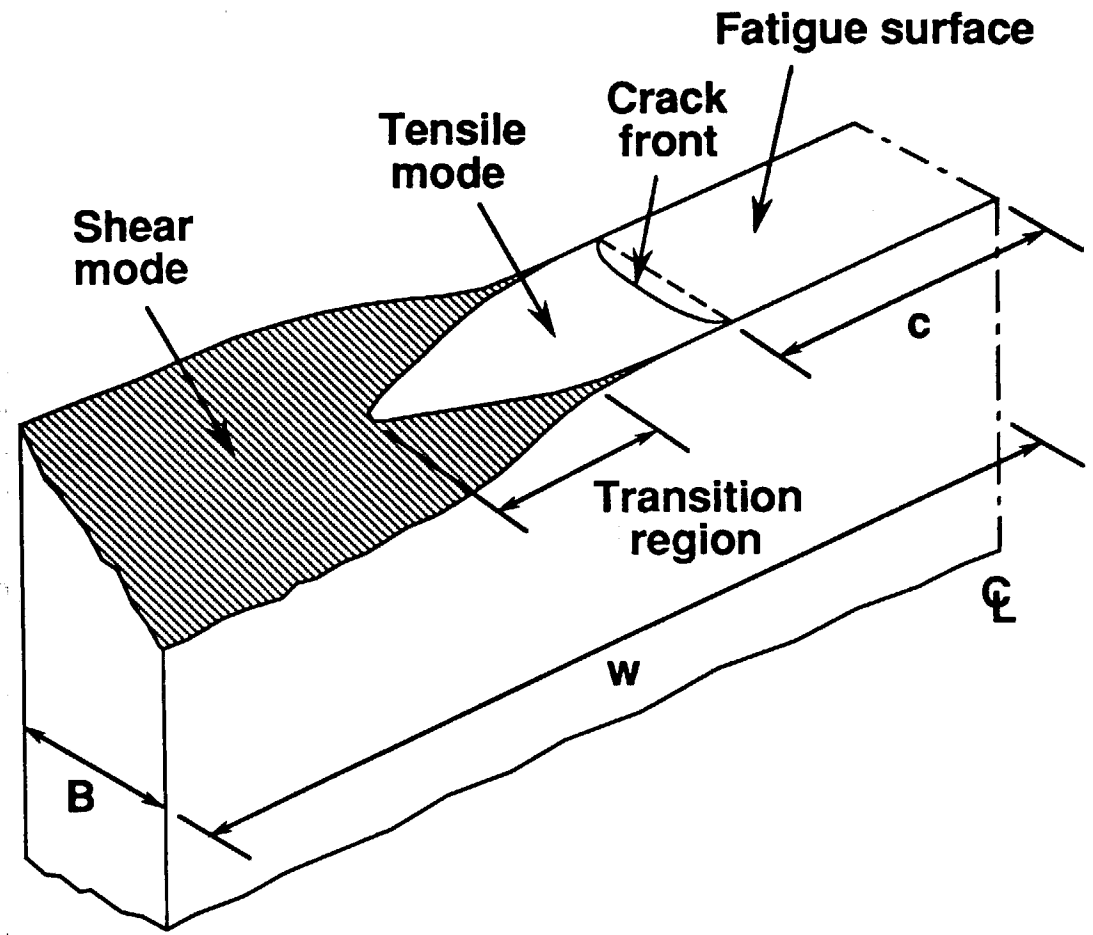

Figure 2.- Fatigue and fracture crack surfaces showing transition from tensile to shear mode crack growth.

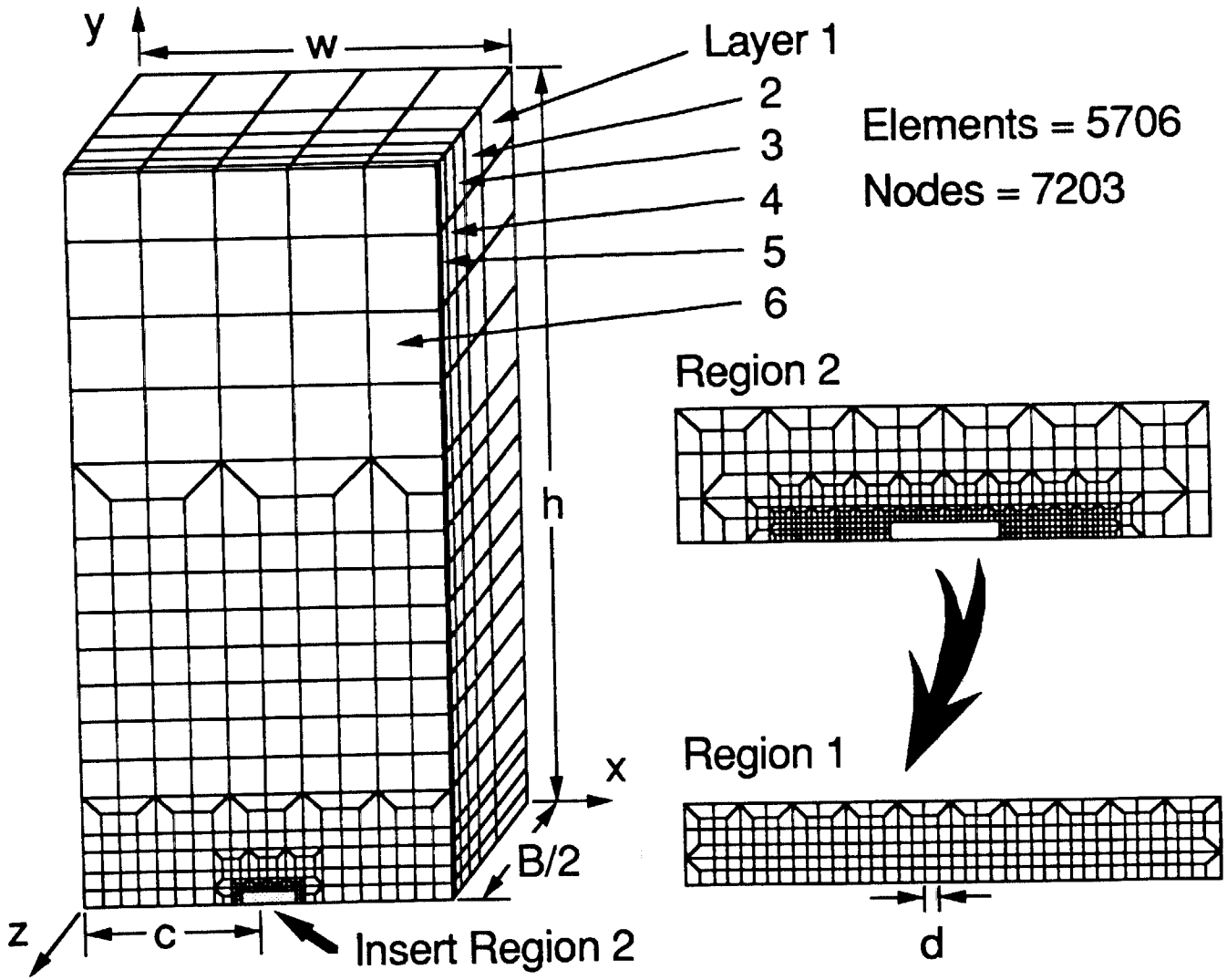

Figure 3.- Finite-element model of middle-crack tension specimen with c/w = 0.5.

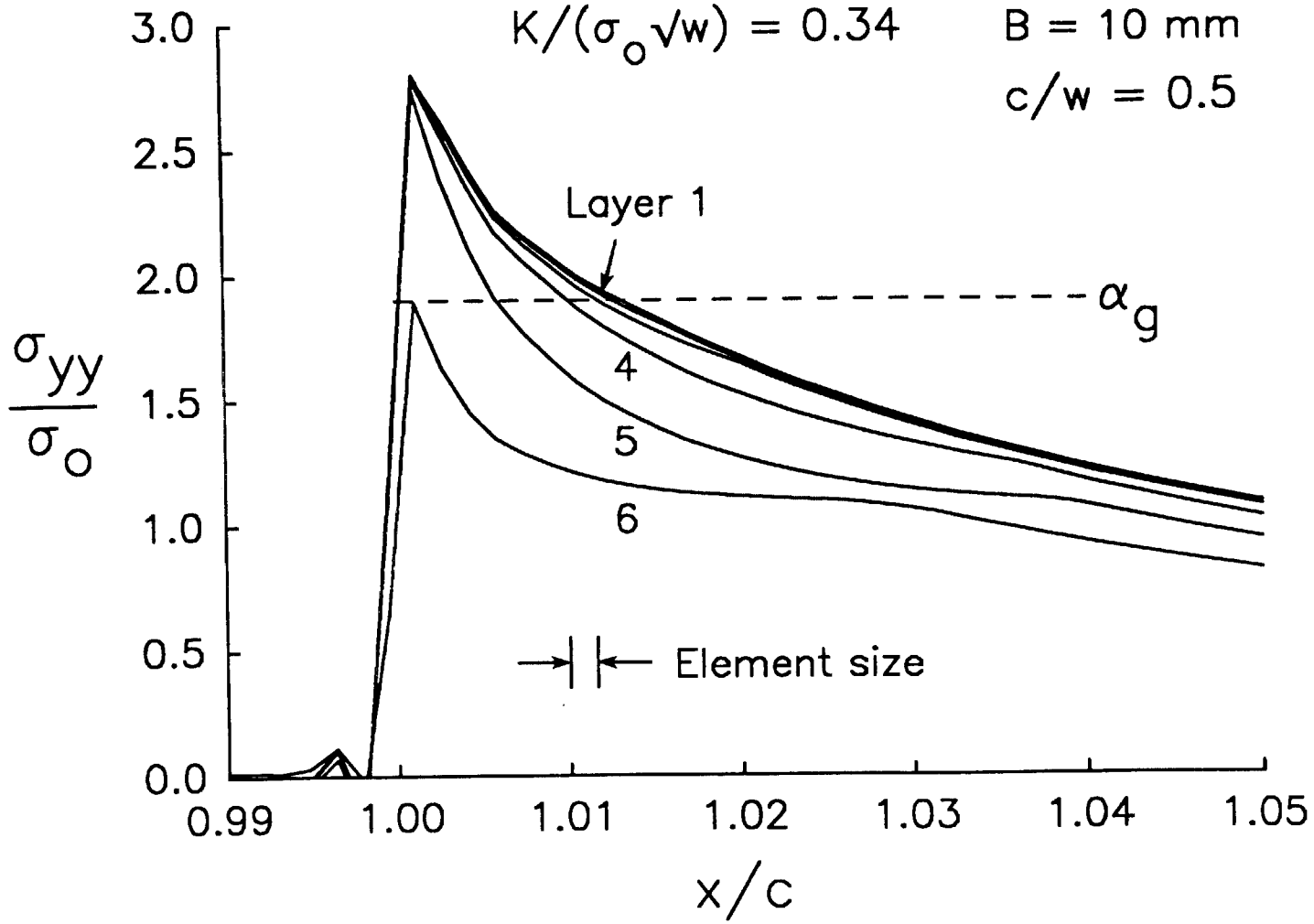

Figure 4.- Normal stresses near the crack front in thick (B = 10 mm) material.

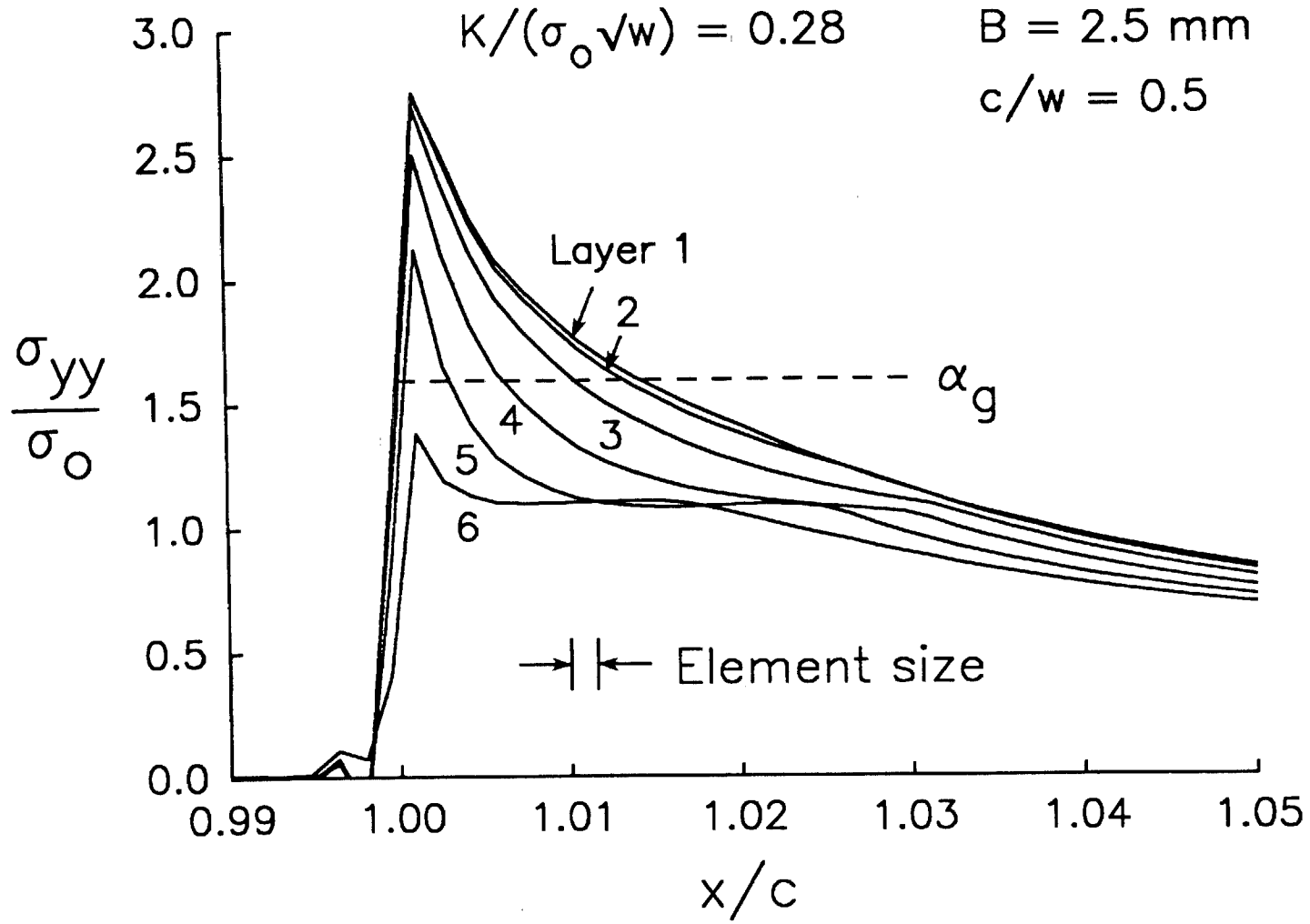

Figure 5.- Normal stresses near the crack front in thin (B = 2.5 mm) material.

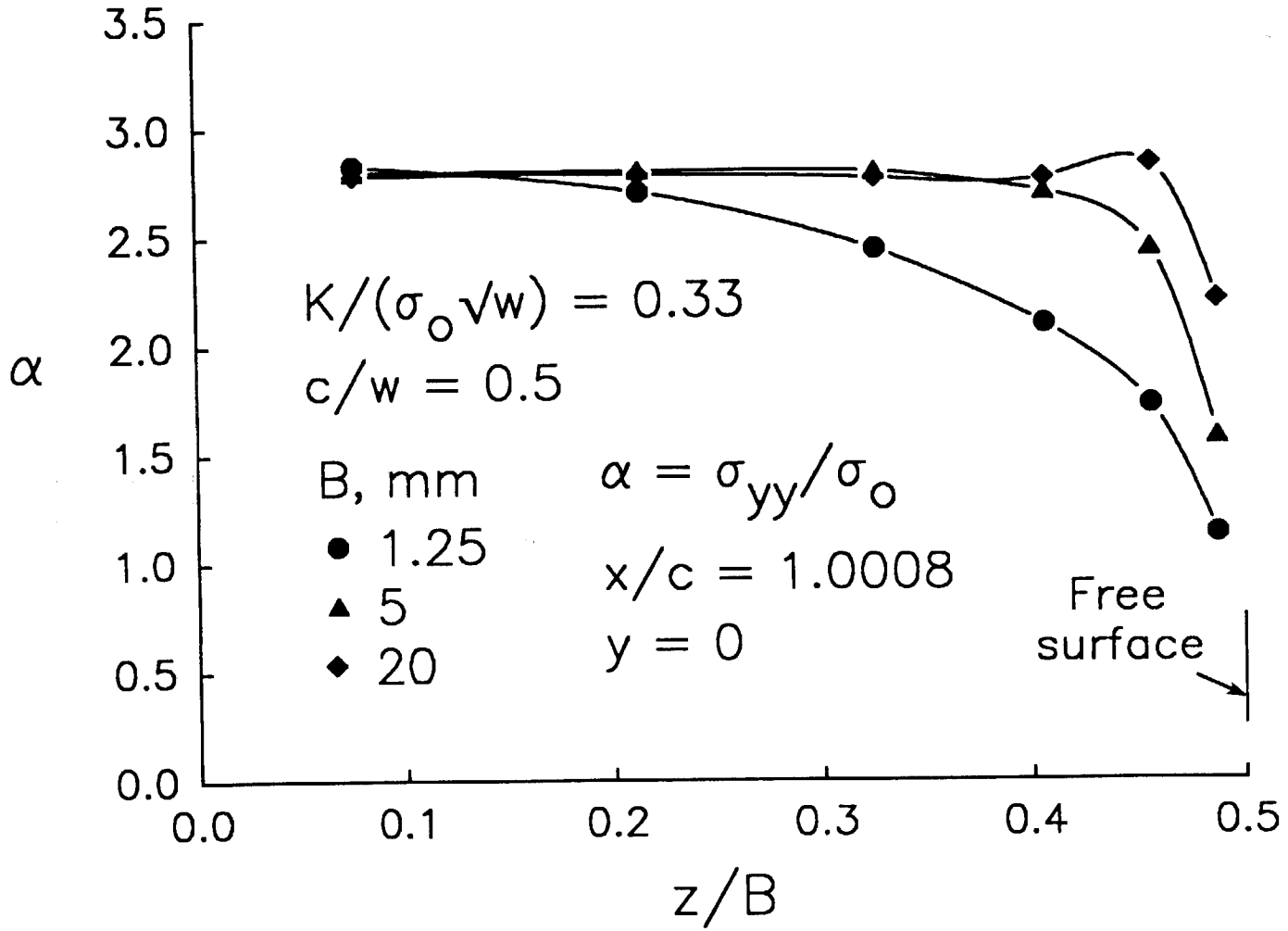

Figure 6.- Normal-stress constraint factor, α, along the crack front for various thicknesses.

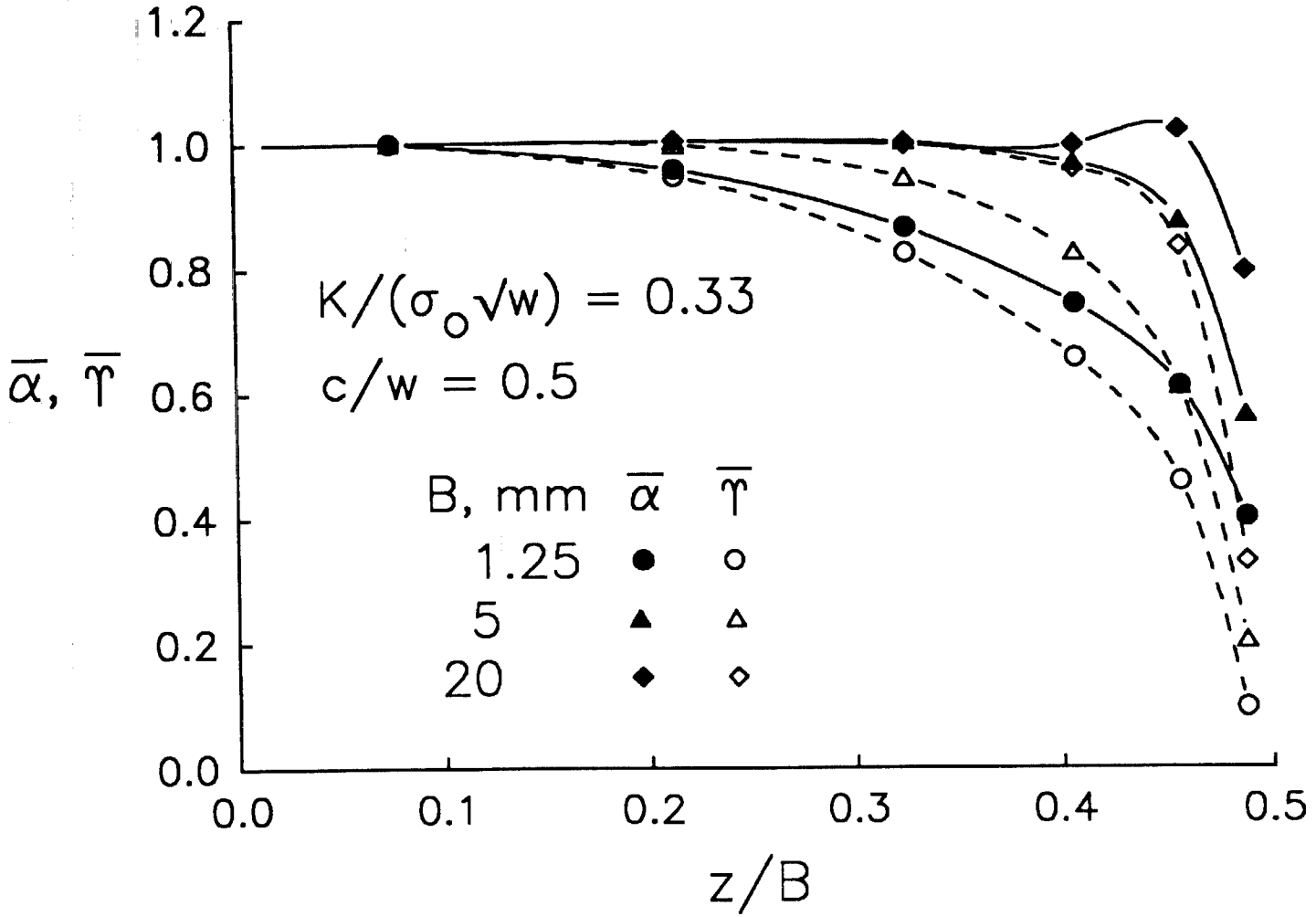

Figure 7.- Comparison of normalized normal- and tangential-stress constraint factors along the crack front for various thicknesses.

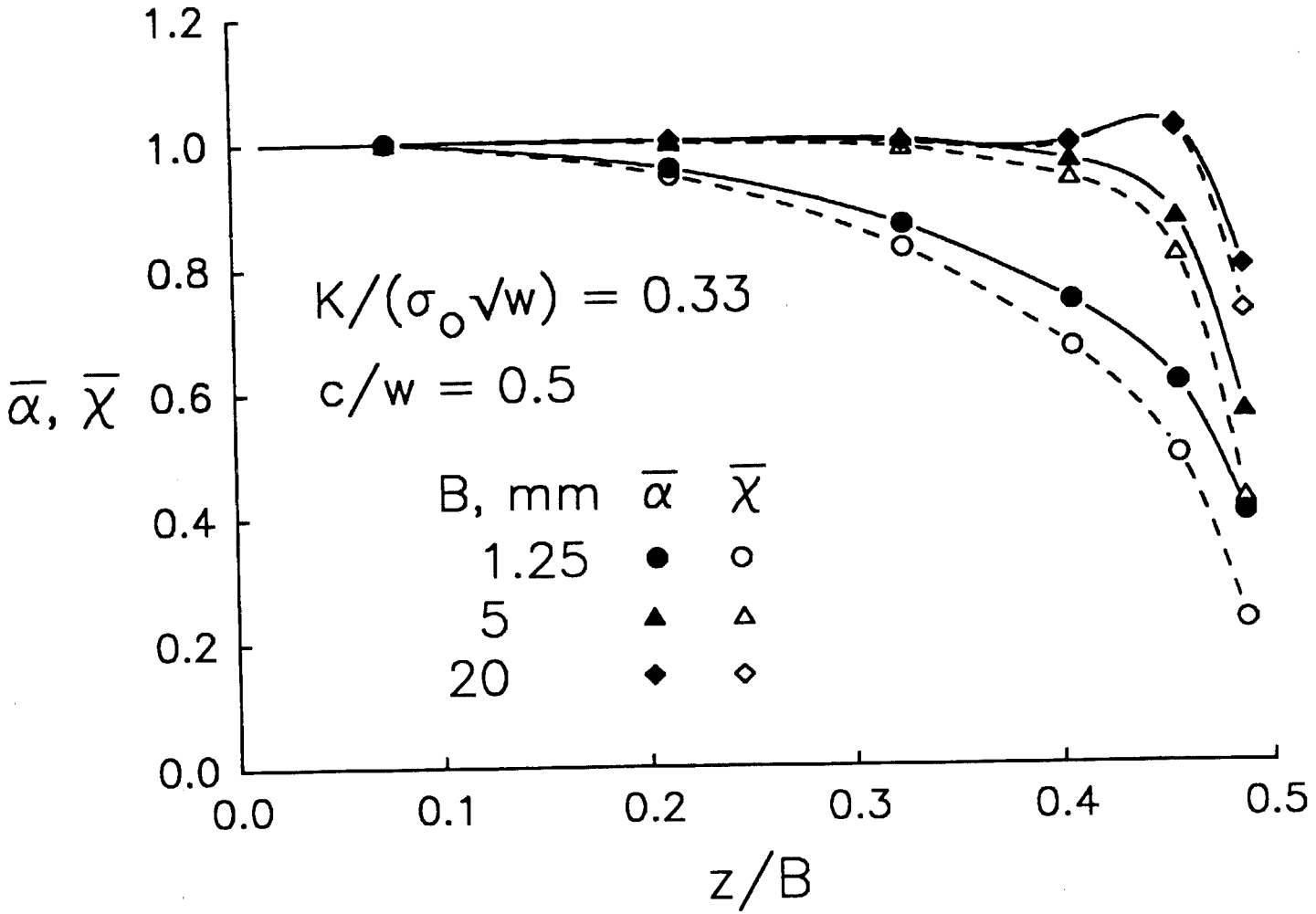

Figure 8.- Comparison of normalized normal- and hydrostatic-stress constraint factors along the crack front for various thicknesses.

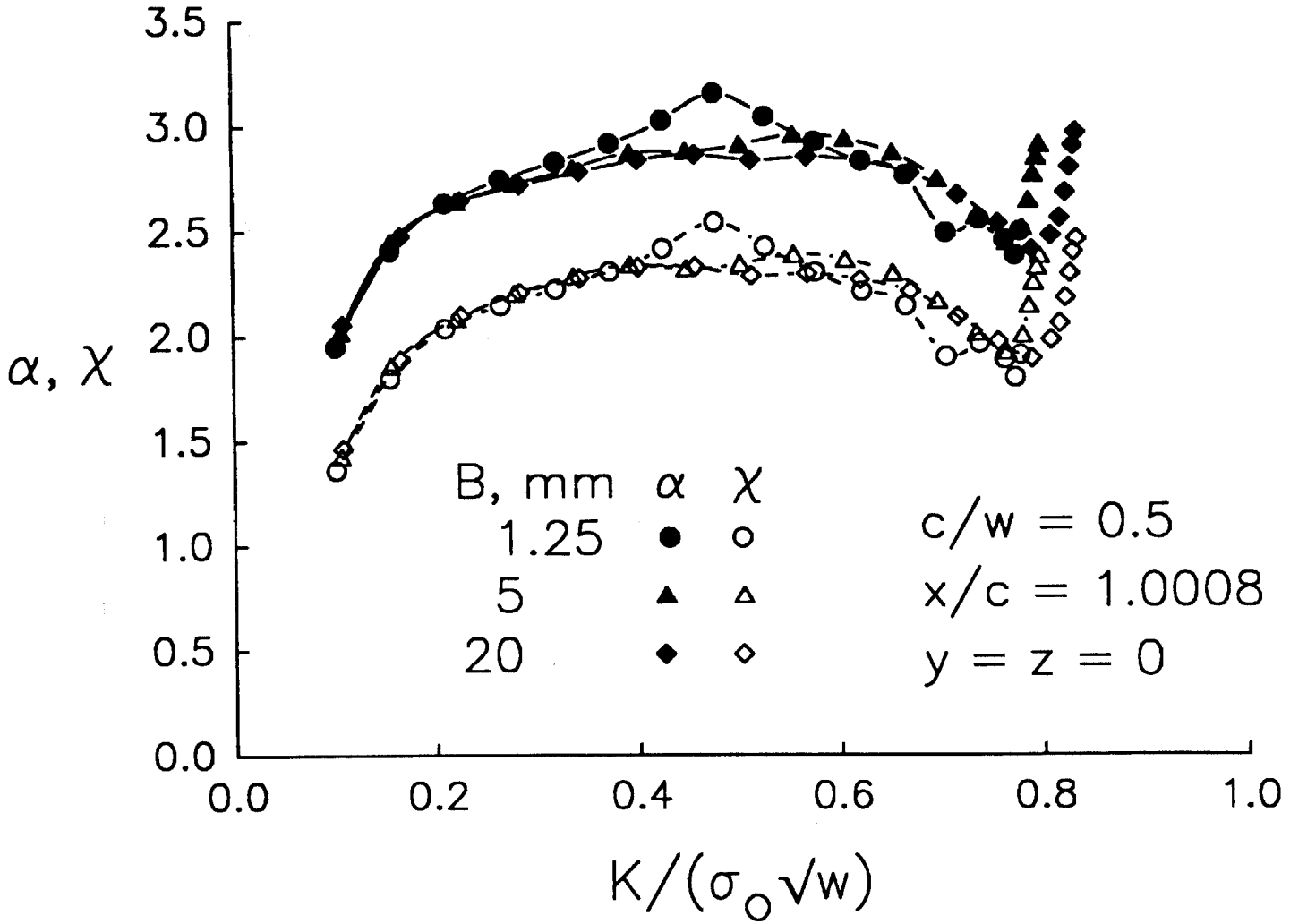

Figure 9.- Comparison of normal- and hydrostatic-stress constraint factors at the mid-plane of various thicknesses as a function of applied $K/(\sigma_o\sqrt{w})$ levels.

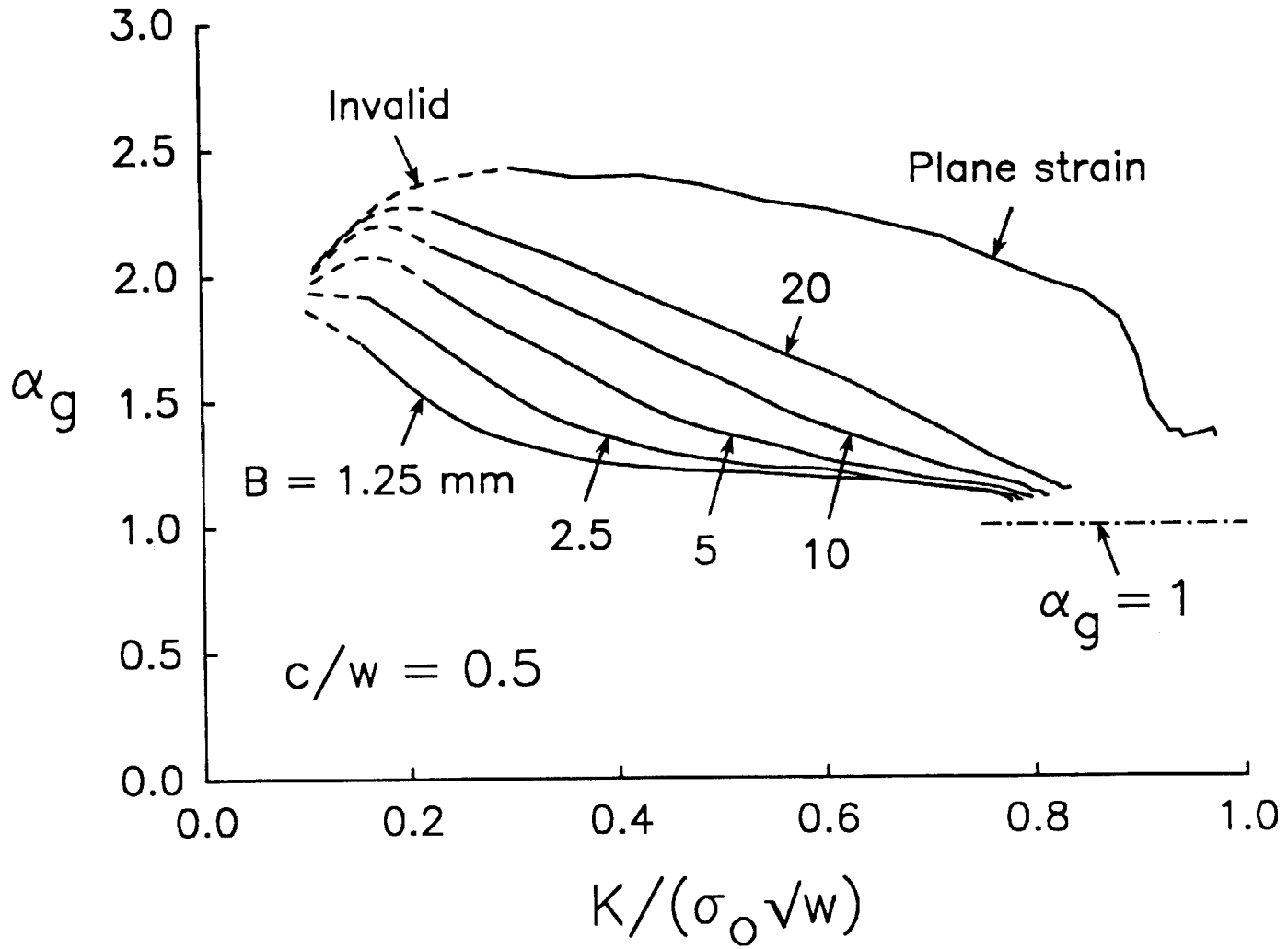

Figure 10.- Global constraint factor, α_g, as a function of applied $K/(\sigma_o\sqrt{w})$ levels for various plate thicknesses with c/w = 0.5.

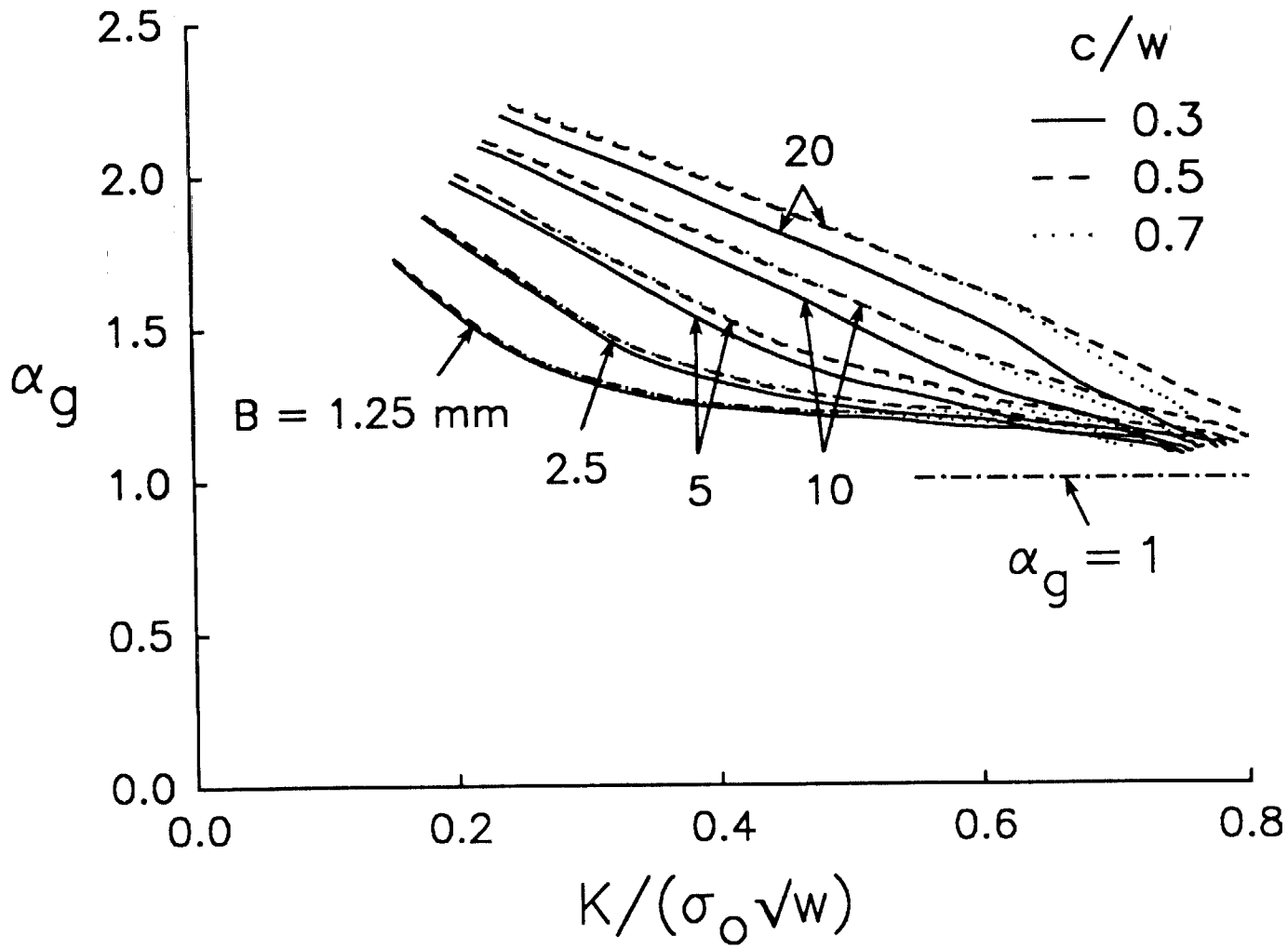

Figure 11.- Global constraint factor, α_g, as a function of applied $K/(\sigma_o\sqrt{w})$ levels for various plate thicknesses and c/w ratios.

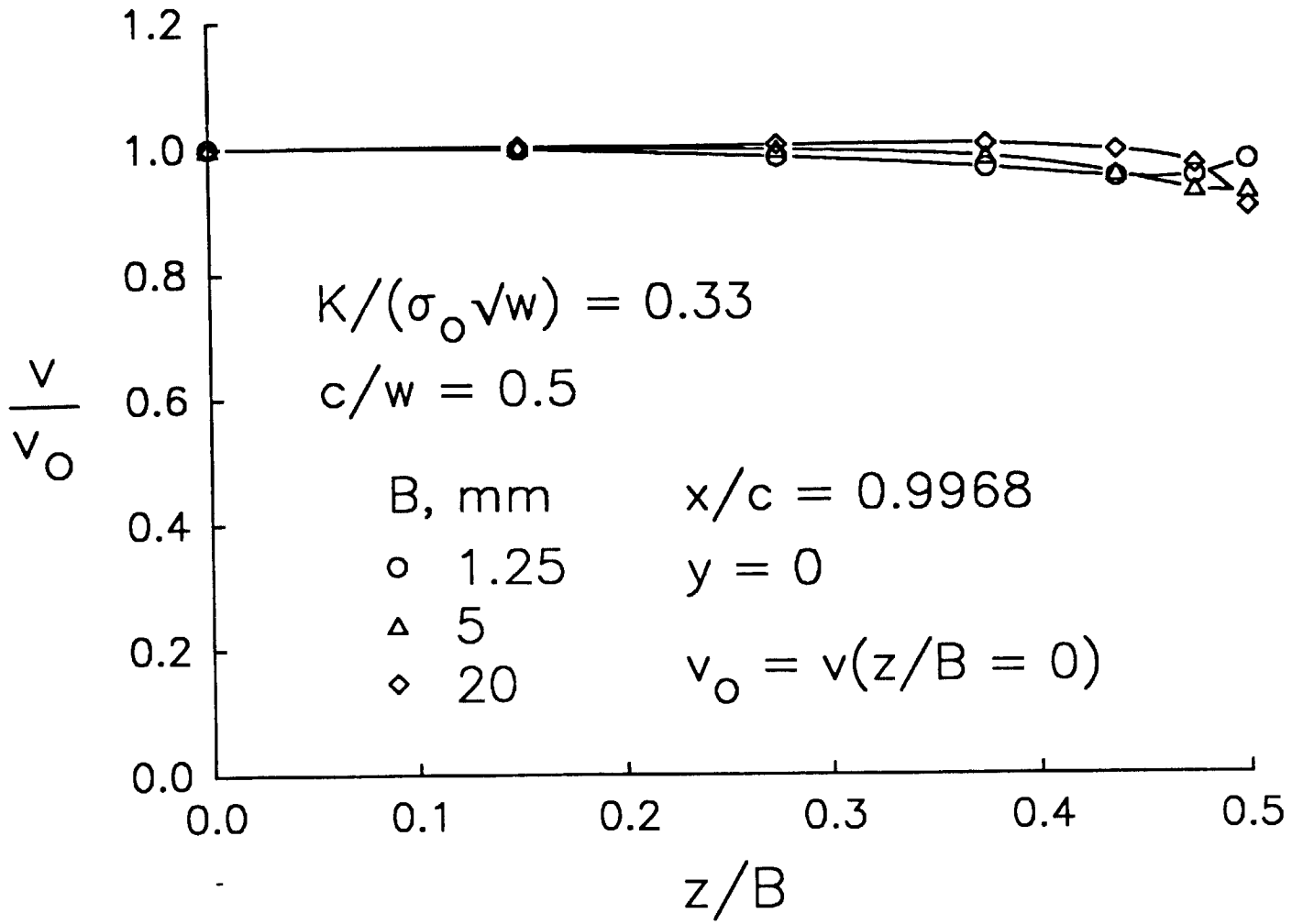

Figure 12.- Normalized crack-tip-opening displacements along the crack-front for various plate thicknesses at an applied $K/(\sigma_o\sqrt{w})$ level of 0.33.

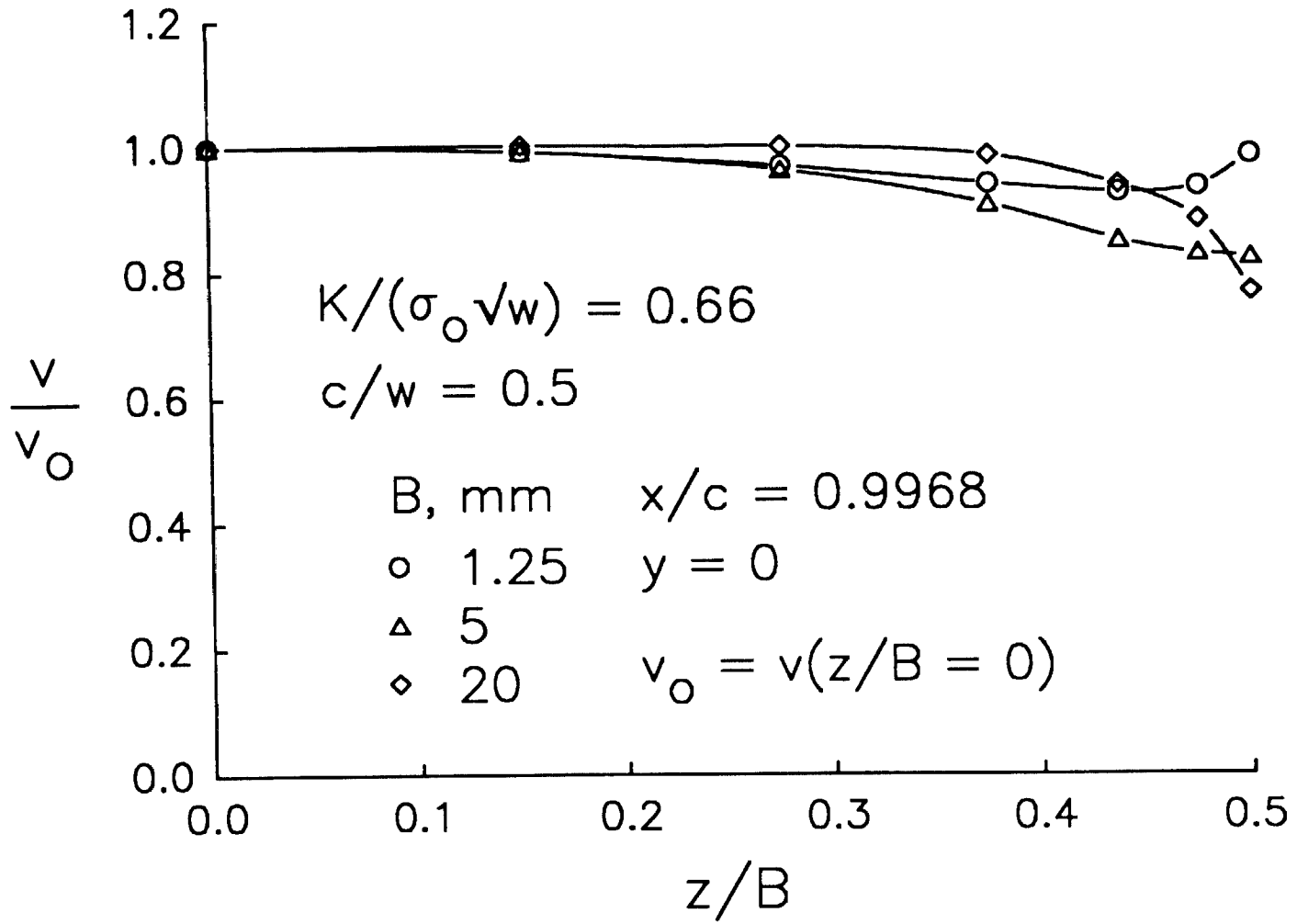

Figure 13.- Normalized crack-tip-opening displacements along the crack-front for various plate thicknesses at an applied $K/(\sigma_o\sqrt{w})$ level of 0.66.

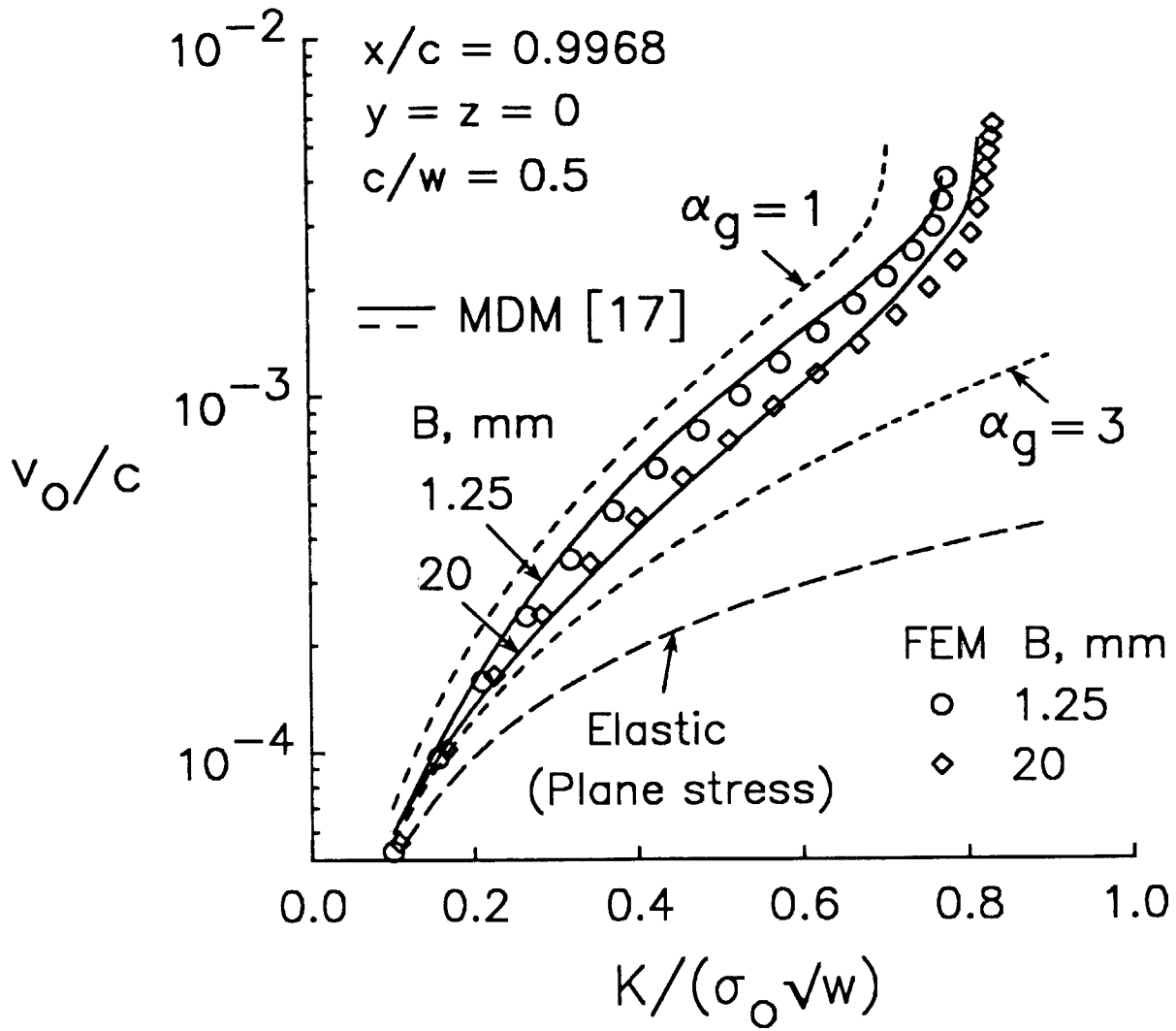

Figure 14.- Comparison of crack-tip-opening displacements at the mid-plane of a thin sheet and thick plate as a function of applied $K/(\sigma_o\sqrt{w})$ levels from various methods.

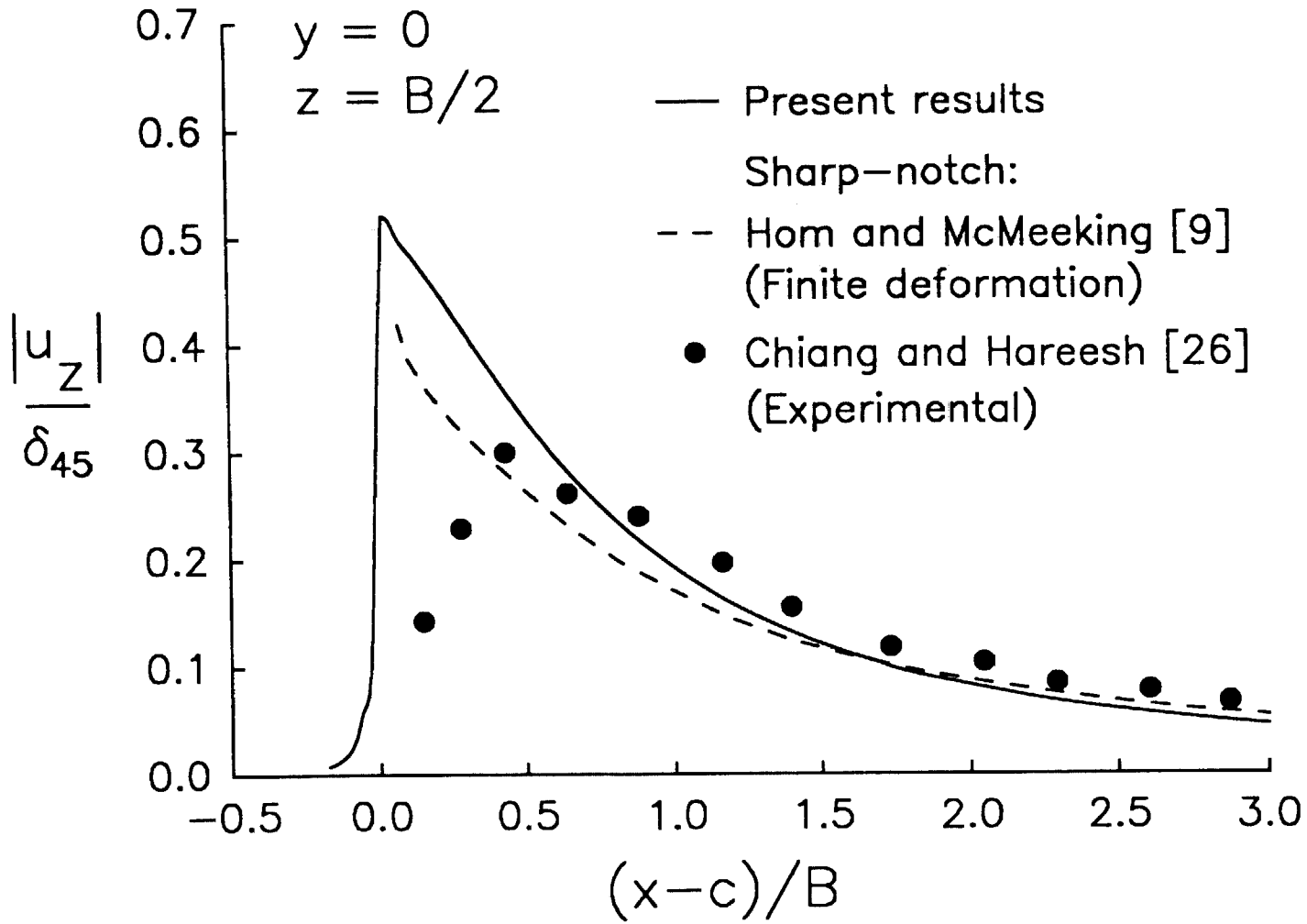

Figure 15.- Comparison of out-of-plane displacements predicted by two finite-element analyses and measured experimentally on a thin-sheet specimen with a sharp notch.

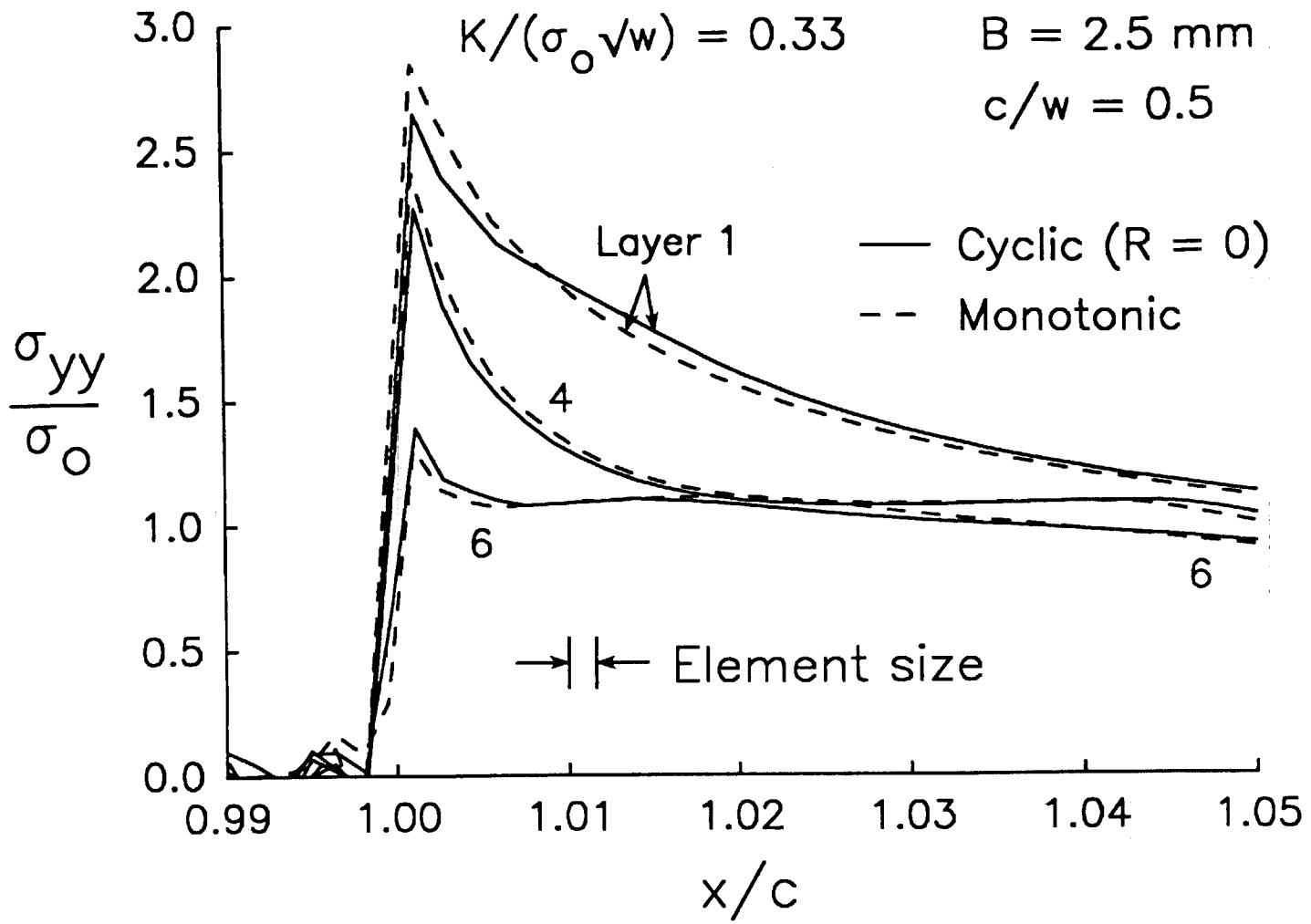

Figure 16.- Normal stresses around crack front under monotonic and cyclic loading on a thin sheet under an applied $K/(\sigma_o\sqrt{w})$ level of 0.33.

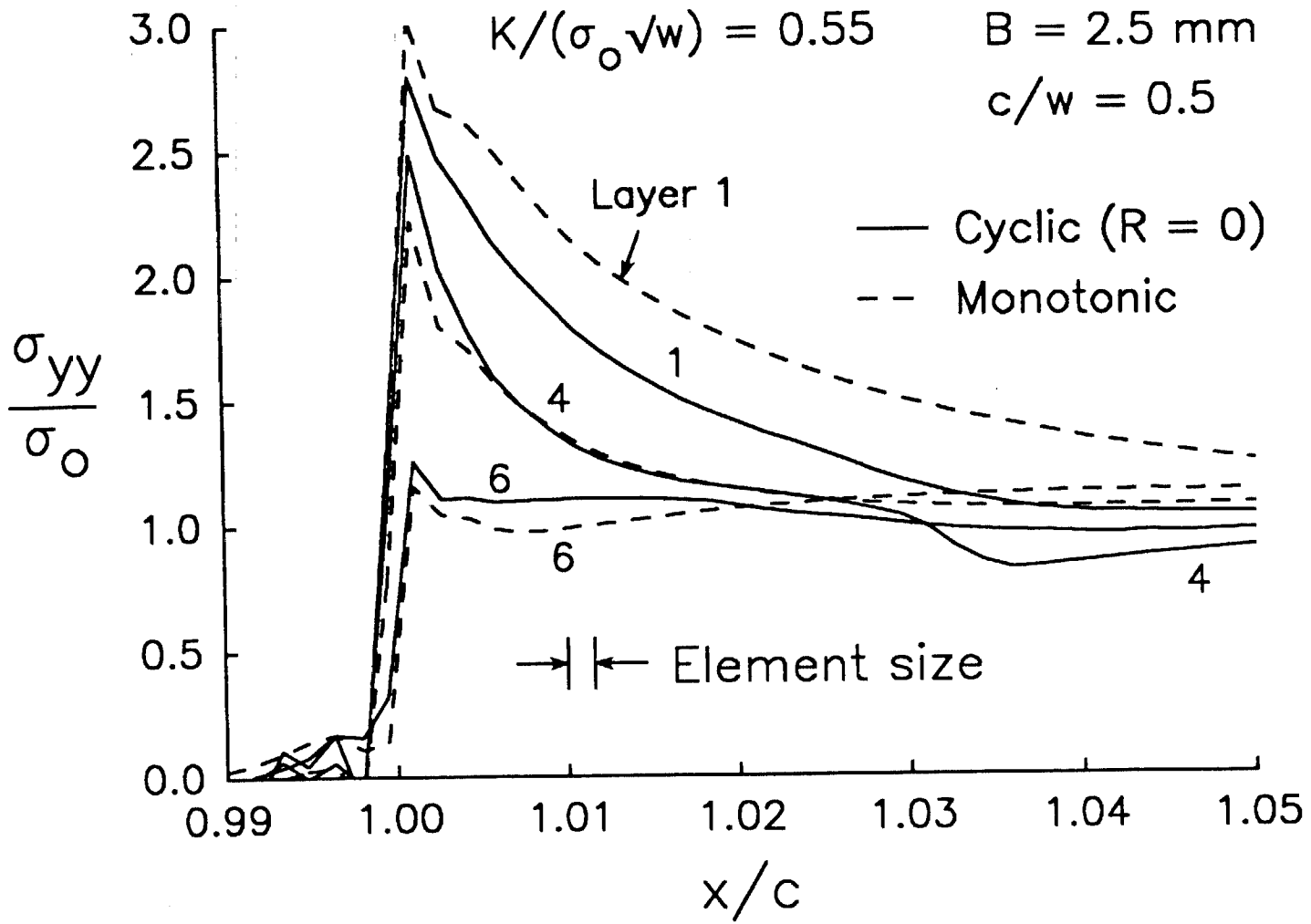

Figure 17.- Normal stresses around crack front under monotonic and cyclic loading on a thin sheet under an applied $K/(\sigma_o\sqrt{w})$ level of 0.55.

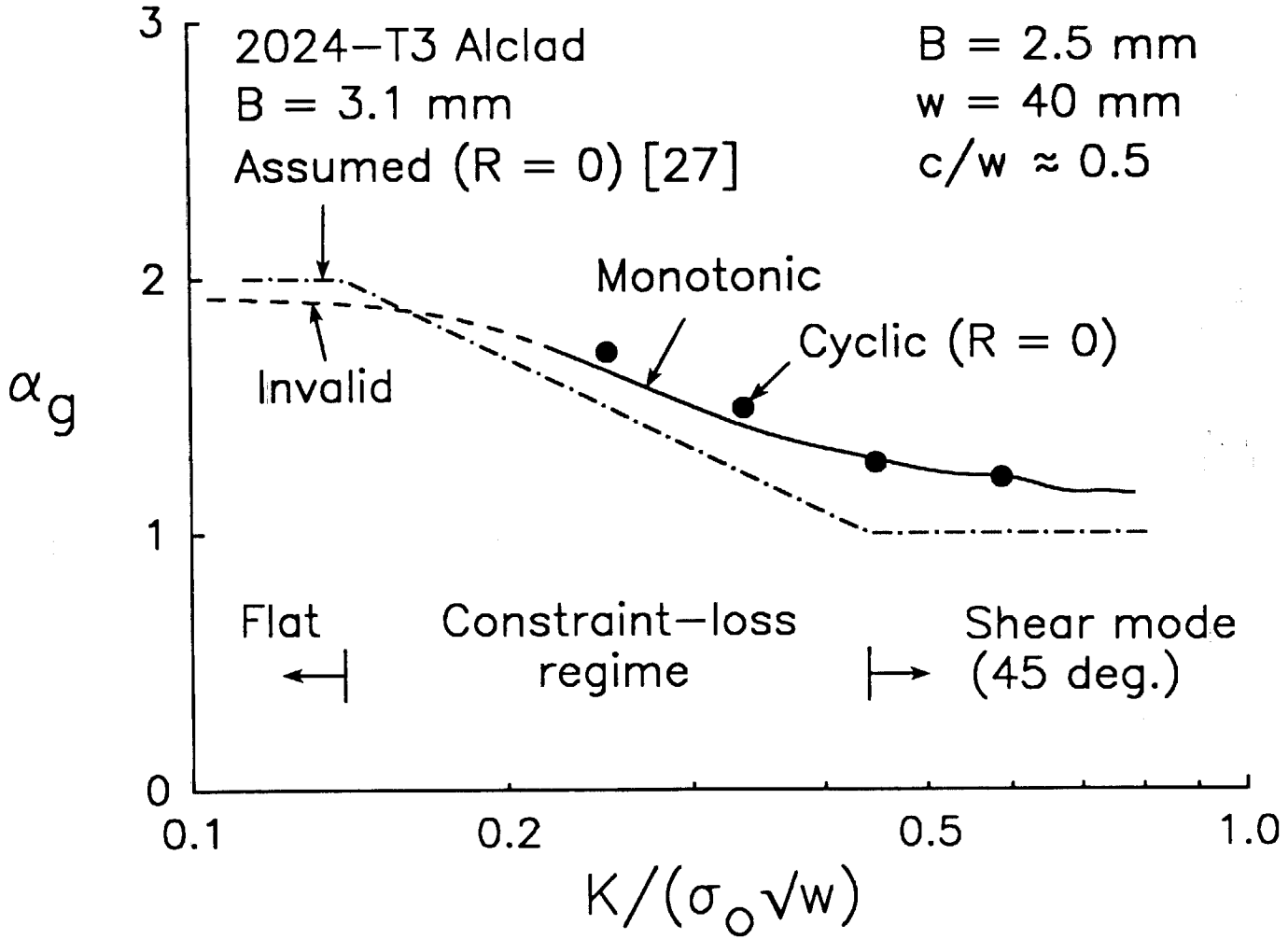

Figure 18.- Comparison of global constraint factors for monotonic and cyclic loading with an assumed constraint variation for a thin sheet as a function applied $K/(\sigma_o\sqrt{w})$ levels.

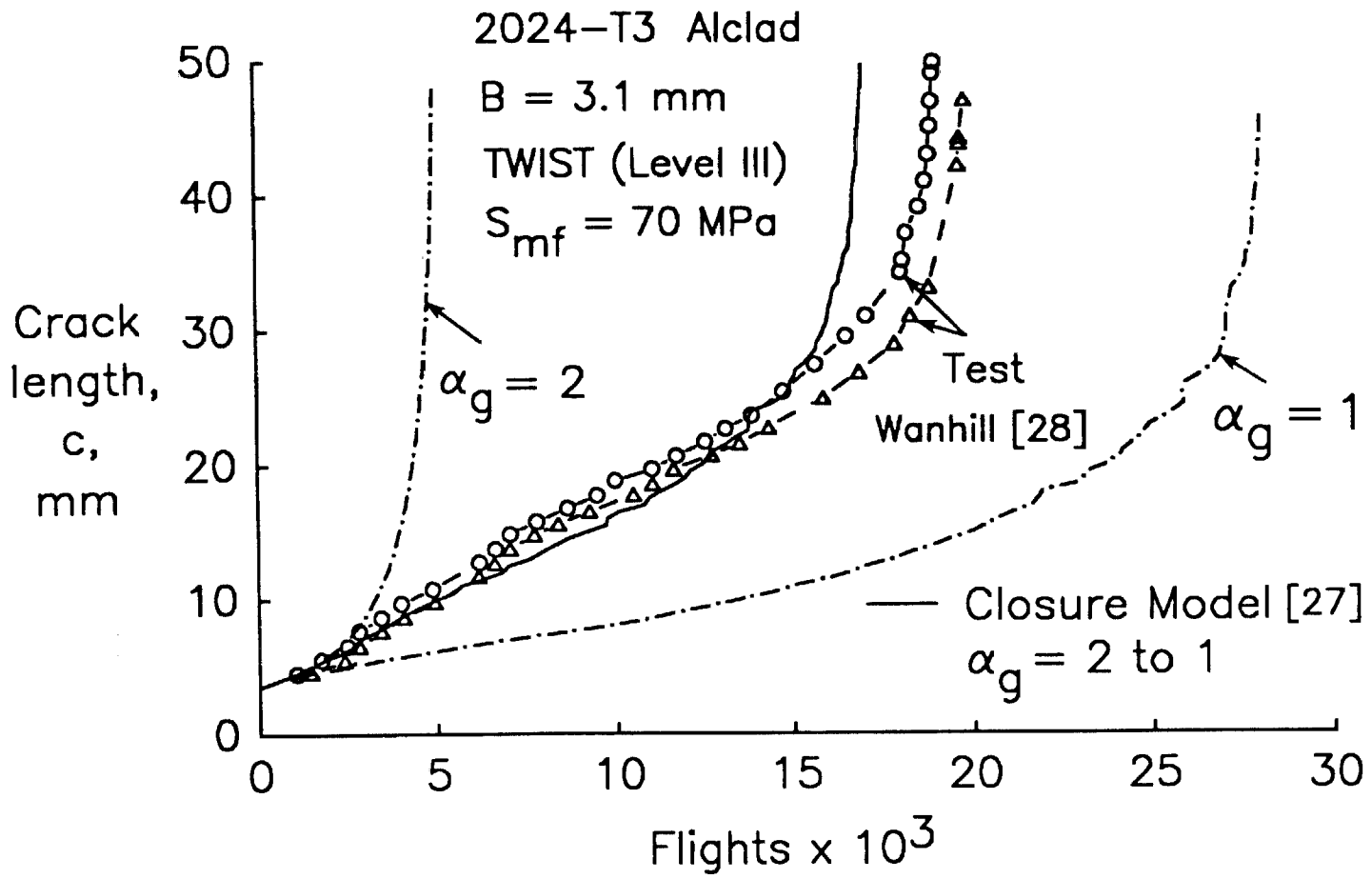

Figure 19.- Comparison of measured and calculated crack-length-against-flights for 3.1 mm-thick aluminum alloy under TWIST (Level III) loading.

REPORT DOCUMENTATION PAGE

Form Approved
OMB No. 0704-0188

1. AGENCY USE ONLY (Leave blank)	2. REPORT DATE	3. REPORT TYPE AND DATES COVERED
	January 1993	Technical Memorandum

4. TITLE AND SUBTITLE

Three-Dimensional Elastic-Plastic Finite-Element Analyses of Constraint Variations in Cracked Bodies

5. FUNDING NUMBERS

505-63-50-04

6. AUTHOR(S)

J. C. Newman, Jr., C.A. Bigelow, and K.N. Shivakumar

7. PERFORMING ORGANIZATION NAME(S) AND ADDRESS(ES)

NASA Langley Research Center
Hampton, VA 23681-0001

8. PERFORMING ORGANIZATION REPORT NUMBER

9. SPONSORING / MONITORING AGENCY NAME(S) AND ADDRESS(ES)

National Aeronautics and Space Administration
Washington, DC 20546-0001

10. SPONSORING / MONITORING AGENCY REPORT NUMBER

NASA TM-107704

11. SUPPLEMENTARY NOTES

Newman and Bigelow: Langley Research Center, Hampton, VA; Shivakumar: North Carolina A&T State University, Greensboro, NC

12a. DISTRIBUTION / AVAILABILITY STATEMENT

Unclassified - Unlimited

Subject Category - 39

12b. DISTRIBUTION CODE

13. ABSTRACT *(Maximum 200 words)*

Three-dimensional elastic-plastic (small-strain) finite-element analyses were used to study the stresses, deformations, and constraint variations around a straight-through crack in finite-thickness plates for an elastic-perfectly plastic material under monotonic and cyclic loading. Middle-crack tension specimens were analyzed for thicknesses ranging from 1.25 to 20 mm with various crack lengths. Three local constraint parameters, related to the normal, tangential, and hydrostatic stresses, showed similar variations along the crack front for a given thickness and applied stress level. Numerical analyses indicated that cyclic stress history and crack growth reduced the local constraint parameters in the interior of a plate, especially at high applied stress levels. A global constraint factor α_g was defined to simulate three-dimensional effects in two-dimensional crack analyses. The global constraint factor was calculated as an average through-the-thickness value over the crack-front plastic region. Values of α_g were found to be nearly independent of crack length and were related to the stress-intensity factor for a given thickness.

14. SUBJECT TERMS

Cracks; Finite-element analysis; Plasticity; Plane strain; Stresses; Displacements; Fracture mechanics

15. NUMBER OF PAGES

43

16. PRICE CODE

A03

17. SECURITY CLASSIFICATION OF REPORT	18. SECURITY CLASSIFICATION OF THIS PAGE	19. SECURITY CLASSIFICATION OF ABSTRACT	20. LIMITATION OF ABSTRACT
Unclassified	Unclassified		